NASA TECHNICAL NOTE

NASA TN D-3305

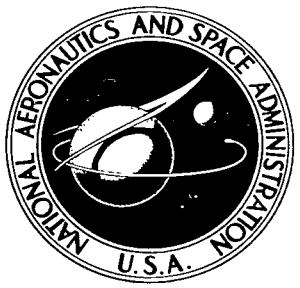

HUMAN TRANSFER FUNCTIONS IN MULTI-AXIS AND MULTI-LOOP CONTROL SYSTEMS

by James J. Adams, Hugh P. Bergeron, and George J. Hurt, Jr.

Langley Research Center
Langley Station, Hampton, Va.

NATIONAL AERONAUTICS AND SPACE ADMINISTRATION • WASHINGTON, D. C. • APRIL 1966

HUMAN TRANSFER FUNCTIONS IN MULTI-AXIS AND MULTI-LOOP CONTROL SYSTEMS

By James J. Adams, Hugh P. Bergeron, and George J. Hurt, Jr.

Langley Research Center
Langley Station, Hampton, Va.

NATIONAL AERONAUTICS AND SPACE ADMINISTRATION

For sale by the Clearinghouse for Federal Scientific and Technical Information
Springfield, Virginia 22151 – Price $0.65

HUMAN TRANSFER FUNCTIONS IN MULTI-AXIS AND MULTI-LOOP CONTROL SYSTEMS

By James J. Adams, Hugh P. Bergeron,
and George J. Hurt, Jr.
Langley Research Center

SUMMARY

Measurements were made of the response of a human pilot in multi-axis tracking tasks. These measurements are the gains in the transfer function of the pilot and the performance measure, root-mean-square error. The measured transfer functions were used to obtain analytically the closed-loop system characteristics. The results show that the pilot changes the response so that the system frequency is reduced as additional axes requiring control are added to the work load. It is shown that these results can be correlated with a theory that the pilot has a given maximum information processing capacity.

These measured multi-axis response characteristics were used to obtain a quantitative description of the characteristics of a multi-loop manually controlled guidance system. The time history of the manually controlled system can be reproduced by using two linear analog models, one for each loop, arranged in series, to represent the pilot. Measurements made in the multi-axis test can be applied to the inner loop, and the same form of the model with modified gains can be used in the outer loop. It is shown that these pilot models will give an analytical description of the instability that can occur when there is an unexpected damper failure in the system; other useful design information is also obtained from these models.

INTRODUCTION

At the present time, human response data are obtained on manually controlled closed-loop control systems through the use of simulators and the actual vehicle. To allow preliminary analytical design studies of flying qualities and to supplement pilot opinions of flying problems, an extensive effort to determine analytical models for the human pilot is being conducted. Previous studies (refs. 1, 2, and 3) have measured the transfer function of human operators in closed-loop control systems. These studies have covered systems with a wide variety of controlled element dynamics in single-axis tasks, in two-axis tasks with one particular controlled element, and in certain nonlinear systems. The present study extends these measurements to include two- and three-axis tasks, each with two different controlled elements. As in the previous investigations,

the transfer function of the pilot was determined by using a model-matching automatic-parameter tracking method.

Another type of control situation that is encountered is the multi-loop problem, in which two or more variables exist, each of which is dependent on the other. This type of situation is distinguished from the multi-axis problem, in which there can be two or more variables, but which are not dependent. The multi-loop situation is also considered in this report. The particular system studied represents the horizontal translation control contained in the lunar landing task. Time histories of the operation of such a system were obtained by using a fixed-base simulator, and these time histories were reproduced by using analog models for the pilot. Measurements obtained in the two- and three-axis tests were used in the inner or attitude control loop. The outer-loop analog pilot model was of the same form as that used in the inner loop. A trial-and-error method rather than the model-matching method was used to determine the gains of this analog model.

As an example of the use of these analog pilot models in supplementing pilot ratings, the multi-loop pilot transfer functions were used to study the unstable system characteristics that can occur when there is an unexpected damper failure in the system. Examples of these instabilities were obtained by using the fixed-base simulator, and the corresponding analytical description of these instabilities was also determined.

SYMBOLS

The units used for the physical quantities defined in this report are given both in the U.S. Customary Units and in the International System of Units, SI (ref. 4). The appendix presents factors relating these two systems of units.

g gravity, 32.2 ft/sec^2 (9.81 m/sec^2)

K_1, K_2 nondimensional computer gains

K_3 controlled element static sensitivities, either nondimensional computer gains or dimensional with units as given

s Laplace operator, per second

W_e earth weight of vehicle

x_i desired vehicle translation, ft (m)

x_o actual vehicle translation, ft (m)

X,Y,Z roll, pitch, and yaw freedom; subscript indicates total number of degrees of freedom

x translation, ft (m)

ζ damping ratio

θ pitch attitude angle, deg

θ_i desired vehicle tilt, deg

θ_o actual vehicle tilt, deg

τ nondimensional computer gain

φ roll attitude angle, deg

ψ yaw attitude angle, deg

ω_n undamped natural frequency, radians/sec

A dot over a symbol denotes differentiation with respect to time.

APPARATUS AND TESTS

The task performed in the multi-axis tests was compensatory tracking of a random disturbance. This task was performed by using a fixed-base simulator with a three-axis eight-ball instrument for the display, and a two-axis side-arm controller and rudder pedals for control. A photograph of the simulator is shown in figure 1. The diameter of the eight ball was $4\frac{1}{2}$ inches (11.4 cm) and the subject was located approximately 28 inches (71 cm) from the instrument panel. Fore-and-aft movement of the side-arm controller operated the pitch motion of the display, side-to-side controller motion operated the roll motion, and the rudder pedals controlled the yaw motion. The side-arm controller had a maximum freedom of movement of $\pm 26^\circ$ in each axis, the freedom of the rudder pedals was $\pm 20^\circ$, and the sensitivity of each control was 1 volt per degree. The simulated controlled element dynamics used in these tests consisted of two rate control systems and two acceleration control systems. The transfer functions for the controlled element dynamics are given in the following table with maximum accelerations and velocities (in units of instrument-display degrees) that will result from a 1° step displacement of the controller or rudder pedals. The gain of the eight ball was 5° per volt.

Dynamics	Maximum acceleration per degree stick deflection, deg/sec^2	Maximum velocity per degree stick deflection, deg/sec
$\frac{0.5}{s(s + 0.5)}$	2.5	5
$\frac{2}{s(s + 1)}$	10	10
$\frac{0.5}{s^2}$	2.5	∞
$\frac{2}{s^2}$	10	∞

These sensitivities provided adequate control for the disturbance used in the tests. The disturbance was obtained by passing the output of a Gaussian noise source through two first-order filters. The amplitude and break frequency for the filtered disturbance were varied during the tests to provide a suitable work load for each test. The break frequencies varied from 0.06 to 0.25 radian per second. The root-mean-square values for the disturbances are given in the following table:

Break point frequency, rad/sec	Root mean square, volts
0.25	9.1
.125	6.1
.06	[a]4.5

[a]Estimated value.

The same disturbance signal was used on each axis of the multi-axis tests.

The eight-ball display was used without an Euler transformation of attitude control torques. The task presented to the pilot was therefore one in which the control torque was to be applied to the gimbal axis of the instrument rather than to an axis system oriented to the reference marks on the instrument. At the same time, the disturbance characteristics were adjusted so that system error of less than 30° (except for widely spaced incidents) occurred in the tests. This arrangement allows the analysis of the pilot's response to be treated as though each axis of the multi-axis system was a separate and uncoupled system. A block diagram that applies to each individual system is shown in sketch (a).

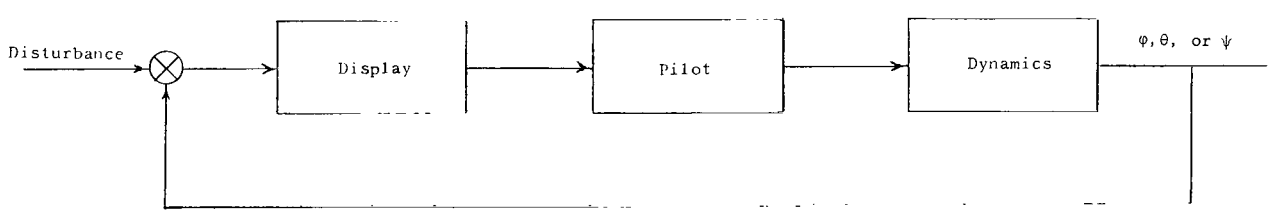

Sketch (a).- Block diagram of single control loop used in multi-axis simulation.

Four NASA test pilots were used as subjects in these tests. The subjects were tested in the pitch, roll, and yaw axes separately, then in the combination of pitch and roll axes, and finally in the pitch, roll, and yaw axes combined. A practice run, which lasted as long as the subject desired, was given before each data acquisition run. Then a 3-minute data run was conducted.

The transfer function of the pilot was obtained by the model-matching automatic-parameter-tracking method described in reference 1. This method uses a model of the form

$$\frac{\text{Output}}{\text{Input}} = \frac{K_1\tau + K_1K_2s}{(\tau + s)^2}$$

constructed with analog computer equipment, and the gains K_1, τ, and K_2 are automatically adjusted to provide the best possible match to the pilot. An illustration of the ability of this scheme to identify a known system is presented in figure 2. In this test the known system was of the same form as that selected for the adjustable model and was given gains of $K_1 = 7.5$, $\tau = 7.5$, and $K_2 = 7.5$. This system, or analog pilot, was placed in a control loop with dynamics of $\frac{K_3}{s(s + 1)}$. The adjustable model was given initial values of gain of $K_1 = 5$, $\tau = 10$, and $K_2 = 5$. The figure shows that the adjustable model quickly matches the known model and arrives at the desired gain values. Other examples in which the adjustable model is required to track time varying gains in a known system are presented in reference 2.

In the multi-loop experiments, a simulator was devised to represent the horizontal translation guidance system, which is a part of the lunar landing maneuver. This system consists of a vehicle supported by a rocket alined with the vertical body axis of the vehicle. Translation is performed by tilting the vehicle until the desired horizontal acceleration is achieved. There is no damping of this horizontal motion in the simulation, only horizontal translation was studied; vertical motion and thrust control were not simulated. A pictorial diagram of the problem is shown in sketch (b). The simulated motion was displayed to the subject with an x,y plotter and a small dial meter. The tilting of the vehicle was displayed on the meter, which was mounted on the moving carriage of the x,y plotter. The horizontal movement of the plotter displayed the horizontal movement of the vehicle. A photograph of the simulator with the x,y plotter set upright in front of the subject is shown in figure 3. The subject exercised control by moving the control stick from side to side.

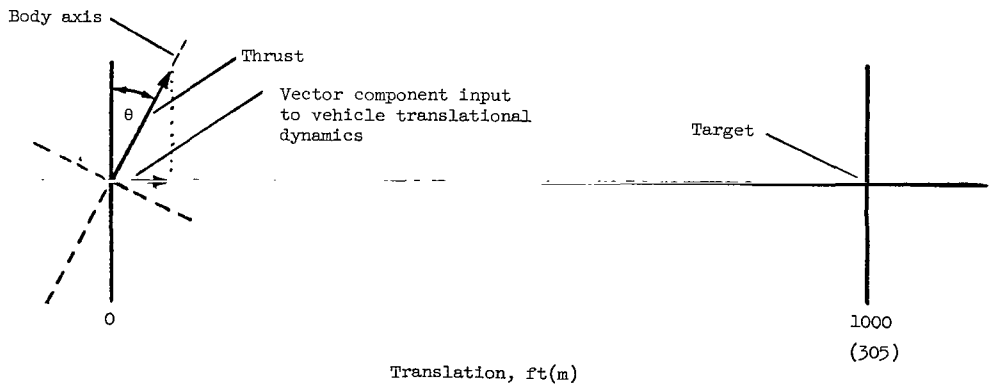

Sketch (b).- Pictorial diagram of double-loop simulation.

Two different inner-loop vehicle transfer functions were simulated $\frac{K_3}{s^2}$ and $\frac{K_3}{s(s + 1)}$. The sensitivity was adjusted so that 1 degree of stick deflection

produced 2.54 deg/sec^2 of displayed tilt angle. This tilt angle is the input to the outer-loop dynamics, which was $\frac{K_3}{s^2}$. The sensitivity of the outer loop was adjusted to simulate the particular task of translating a vehicle over the lunar surface as follows: The thrust required to hover over the moon is one-sixth of the earth weight of the vehicle W_e. It was assumed that the thrust remained constant at this value. The expression for horizontal acceleration is then given by the formulas:

$$\ddot{x} = \frac{W_e}{6} \frac{g}{W_e} \sin \theta = 5.36 \text{ ft/sec}^2 \sin \theta = 1.63 \text{ m/sec}^2 \sin \theta$$

The small angle approximation was used to linearize this relationship, so that the control sensitivity of the outer loop was

$$\frac{\ddot{x}}{\theta} \approx \frac{5.36 \text{ ft/sec}^2}{\text{rad}} = \frac{1.63 \text{ m/sec}^2}{\text{rad}}$$

Therefore the value of acceleration due to thrust K_3 for the outer loop is 5.36 (1.63) when considered in terms of ft/sec^2 (m/sec^2). The outer-loop simulator display sensitivity was such that 1 inch (2.54 cm) of motion of the x,y plotter represented 160 feet (48.8 m) of vehicle travel.

The problem given to the subject in the multi-loop simulation was to translate approximately 1,000 feet (305 m). The subjects operated the system so that this translation was completed in approximately 30 seconds. However, the tests were continued for approximately 2 minutes to provide a good definition of the hovering maneuver which followed the translation.

The multi-loop experiments were also extended to include a third loop, which was displayed to the pilot by the vertical motion of the x,y plotter. Engineers only were used as subjects in the triple-loop experiments. This triple-loop problem is considered in the abstract sense and is not directly related to any physical problem. Variations in dynamics were tried in both the double- and triple-loop problems. Various controlled element control sensitivities were also investigated in the double-loop system to determine the effect of changing this variable.

RESULTS AND DISCUSSION

Multi-axis experiments.- Sample time histories taken from the multi-axis investigation are presented in figures 4 to 11. The measured pilot gains and the closed-loop system characteristics for all subjects are given in table I. The time histories show good agreement with the time varying results presented in reference 2. In the single-axis tests, the measured gains are, in general, constant with time whereas in the two- and three-axis tests, the gain K_1,

particularly in the roll and yaw axes, drops to low values or to zero for brief periods of time. It is felt that these reduced values represent periods when the pilot has dropped all attention from that particular axis.

Another result observed in these tests and not recognized in the results of reference 2 is the reduction in system natural frequency that occurs as additional axes for control are added to the pilot's work load. These results are evident from the closed-loop frequencies ω_n presented in the tables. It can be seen that in all cases the closed-loop frequencies for a given axis are reduced when one or more axes are added. These changes in frequency are also apparent in the sample time histories. The root-mean-square values of system error and the normalized error, which was obtained by dividing the root-mean-square system error by the root-mean-square value of the disturbance, show a corresponding increase as the system natural frequency decreases.

As an explanation for this reduction in system natural frequency, a theory is proposed that it is the effect of a maximum information processing capacity existing in the pilot. It is assumed that the pilot uses his maximum capacity in each test and when this capacity must be shared there is a reduction in the information processing devoted to each axis or channel.

Shannon's theorem (ref. 5) for channel capacity is given by the equation

$$c = \omega \log_2 \left(1 + \frac{S}{N}\right) \text{ bits per second}$$

where c is the information capacity of channel, ω is the bandwidth of channel, S is the average signal power, and N is the average noise power.

In the present investigation, the logarithmic quantity was found to be nearly constant. Changes in information rate showed up almost entirely as changes in system frequency. Since for this investigation the pilot determines the natural frequency of the system, it is proposed that these system frequencies correspond to the pilot's information processing capacity.

Therefore, in the present study, the system natural frequency was considered as a measure of channel capacity, and the ratios of system frequency for single-axis control to two-axis control tasks were determined for each subject. These results, together with the average values for all four subjects, are given in table II. This table shows that the system frequency for each variable is reduced by a factor of 0.75 when a second variable is added to the task. Therefore, the total capacity being exhibited by the pilot in a two-axis task appears to increase by a factor of 1.5 over that for a one-axis task.

Reference 6 is a study of the information processing capacity of humans using one- and two-dimensional displays. This reference shows that when the number of dimensions of the display is doubled the ratio of information transmission capacity increases by a factor of 1.5, from 4.4 bits per second to 6.6 bits per second.

The agreement between the results of the present study and that of reference 6 suggests that a relation does exist between the maximum information processing capacity in a human controller and the closed-loop frequency which the human controller will establish in control systems of the type being studied in this investigation. These systems are ones in which the controlled element dynamics do not possess a static stability of their own.

The ratio of approximately 0.7 between the system frequencies of single- and two-axis tasks also indicated that operator channel capacity can be thought of as a vector which has a given magnitude and which is located in an orthogonal coordinate system having the same number of dimensions as the control task. When the dimensions of the task are doubled, such as occurs when the task is changed from a single-axis to a two-axis task, the information capacity applied to each dimension will change as the orthogonal vector components of the original vector. Thus the capacity devoted to each channel will change by a factor of $\sqrt{1/2}$ or 0.707 when going from a single-axis to a two-axis task. Further, when the task is changed from a single-axis task to a three-axis task, the capacity devoted to each dimension will change by a factor of $\sqrt{1/3}$ or 0.576. It can be further determined that the ratio between a two-axis and three-axis task should be 0.815. The additional data given in table II indicate that the measured data agree well with this vector concept for the human's information processing capacity in a closed-loop tracking task. It is also possible that the apparent increase in information capacity in the multi-axis tests resulted from the fact that the same disturbance signal was used in all three axes. However, the pilots upon questioning after the tests stated that as far as could be determined the disturbance signal appeared to be different for each axis of control.

Multi-loop experiments.- A preliminary attempt to reproduce the pilot's response in a multi-loop control task was presented in reference 3. This reproduction was achieved by using analog models for the pilot arranged as shown in block diagram form in sketch (c). This scheme represents the pilot as two separate blocks, one in each loop, arranged in series with the loop of one model system closed around the other model system. An output limiter on the outer-loop analog pilot was also included. This limiter represents the desired limit of the bank angle that the pilot imposes on the control of the attitude of the vehicle. In reference 3, the gains for the outer-loop analog model were found by a trial-and-error procedure and the gains for the inner-loop analog model were taken from measurements made in single-axis compensatory tracking tasks of reference 1. The results were sufficiently good to indicate that, in general, the approach was satisfactory, but it was recognized that improvements

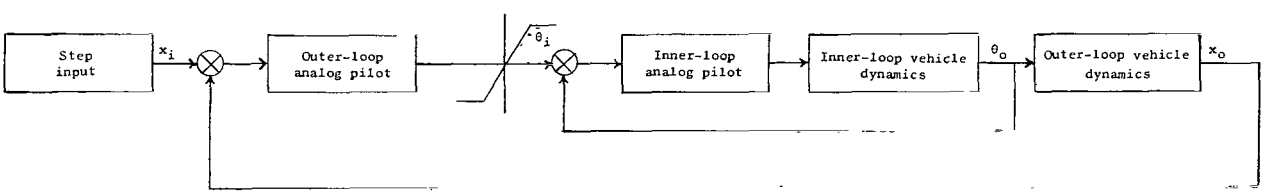

Sketch (c).- Block diagram of double control loop.

in the duplication of the manually controlled tests should be attempted. In particular, it was recognized that the frequency of the inner loop was too high. The multi-axis tests presented in the previous section indicated that, when the human pilot has more to attend to than just a single-axis control problem, it is very reasonable to consider using an analog pilot which produces a lower frequency to represent a human controller.

Piloted simulator tests representative of the translation guidance portion of the lunar landing maneuver were made and these maneuvers were reproduced by using measured data taken from the multi-axis tracking studies for the inner-loop analog pilot. A new determination of the gains for the outer-loop analog pilot was also made.

A typical time history of the piloted simulator tests and the best reproduction achieved by using the analog models of the pilot are presented in figure 12. It can be seen that the reversal in attitude angle, the small overshoot followed by a slow decay to the desired value of translation, and the frequency of the attitude mode of motion are all closely reproduced. The inner-loop analog pilot and associated vehicle dynamics used in obtaining the match to the piloted test were taken from the multi-axis test X_2 of pilot D presented in table I(b). This particular set of measured data was chosen because the system frequency, which it produces, closely matched the vehicle attitude mode of motion frequency observed in the simulator test and because the vehicle lag time constant was approximately the same as that used in the simulator test. The inner-loop dynamics in the simulated test was $\frac{K_3}{s(s + 1)}$. It is felt that other sets of data from table I could also have been used, as is illustrated by the following paragraph, or that sets of data obtained by interpolating the measured data could also have been used. The outer-loop analog pilot gains used in obtaining the match were $K_1 = 0.09$, $\tau = 10$, and $K_2 = 92$.

Analytically determined linear system characteristics are presented in table III(a) for the values of gains used in obtaining the time history in figure 12. Tables III(b) and (c) include two examples using the inner-loop pilot gains measured for pilot J (presented in table I(c)) and the same outer-loop gains used in table III(a). Included in table III are the closed-loop characteristics for the inner-loop alone, for the outer loop with the inner-loop transfer function assumed to be 1, and for the complete system. It can be seen from this table that some coupling does exist between the various modes of motion, since the characteristics of each loop considered separately are different from the system considered as a whole. The damping of the attitude mode of motion appears to be the most sensitive characteristic because it is changed the most.

The gains for the outer-loop analog model given in the previous paragraph provided the best match to the particular manually controlled time history presented in figure 12. Independent variations in these gains were tried also. The gain K_1 determines the frequency of the translation mode of motion. A 50-percent increase in K_1 resulted in an overshoot that was greater than was normally encountered in tests with experienced operators, and a 50-percent reduction resulted in a very sluggish translation response. On the basis of an

overall best match to a typical manually controlled run, the value $K_1 = 0.09$ was judged to be the best value.

Values of τ ranging from 2.5 to infinity were tried also. When the value for τ was changed, K_1 and K_2 were also changed in order to keep the static gain K_1/τ and the lead time constant K_2/τ unchanged. A fairly good match was achieved with all these values of τ. However, on the basis of achieving the best fit to both the low frequency translation mode of motion and the higher frequency attitude mode of motion, the value $\tau = 10$ was selected as providing the best overall match.

Variations in K_2 lead to very noticeable changes in the translation mode of motion, as did K_1 changes, and also affected the attitude mode of motion. At the same time it was known that practiced human controllers would sometimes operate the system in a manner which resulted in a sluggish response in translation. An example of this slower type of response is shown in figure 13 along with a response obtained from an analog model with an outer-loop gain K_2 of 120. On the basis of matching the variation in responses displayed in figures 12 and 13, it is concluded that K_2 can vary from 92 to 120.

The values of gain determined for the outer-loop analog model in this experiment are quite different from those measured in single-axis or multi-axis tracking tests. It is felt that the experiment demonstrates that a linear analog model of the form used, located in the system block diagram as shown, will adequately represent a human operator. However, in other applications, it is felt that the numerical values for the gains may have to be altered.

It should be noted that the square of the frequency, or the product of the two lowest real roots, of the outer loop is a function of the product of the static gain of the pilot transfer function $\frac{K_1}{\tau}$ and the static gain of the controlled element K_3. The values for the present problem are

$$\omega_n^2 \approx \frac{K_1}{\tau} K_3$$

$$(0.17)(0.30) \approx \frac{0.09}{10}(5.36)$$

If the procedure presented in this report is considered for use in other problems that may have a different controlled element control sensitivity, then it is the product $\frac{K_1}{\tau} K_3$ that should be kept constant. This adjustment is the first coarse adjustment that should be made in the K_1 gain to be used in the pilot model. Minor adjustments can then be made to suit the particular case under consideration. These same comments apply to the inner loop.

Multi-loop experiments with unexpected changes in dynamics.- With the use of transfer functions for pilot response it should be possible to obtain a quantitative description of the instability, or pilot induced oscillation, that

can result when an unexpected damper failure occurs. Simulator tests were devised to generate this instability and the system characteristics were calculated with the assumption that the pilot did not change his control response after the damper failure. Similar analyses dealing with aircraft pitch dynamics are presented in references 7 and 8.

In the simulator tests, the previously mentioned multi-loop control task using the x,y plotter and dial display was used. Engineer subjects who were well practiced in performing this task with both $\frac{K_3}{s(s+1)}$ and K_3/s^2 dynamics in the inner loop were used. They were asked to perform the task with the indication that the tests were to be repeat runs using $\frac{K_3}{s(s+1)}$ dynamics in the inner loop. Then the inner-loop dynamics were changed from $\frac{K_3}{s(s+1)}$ to K_3/s^2 during the run, simulating a damper failure. Sample results are shown in figure 14. The point at which the damper failure occurred is indicated in the figure. The typical result was the occurrence of a divergent oscillation or unusually large excursion in attitude angle after the damper failure. After 5 to 10 seconds the system response returned to the type that was usually encountered with K_3/s^2 dynamics in the inner loop.

An analytical determination of the system instability, using the measured gains for pilots D and J and controlled element dynamics taken from tables I(b) and I(c) for the inner-loop and the outer-loop transfer function determined in the previous section, was made and is presented in table III. The table compares the system characteristics with the damper in operation $\left(\text{with } \frac{0.5}{s(s+0.5)}\right.$ inner-loop dynamics for pilot D and $\left.\frac{2}{s(s+1)} \text{ inner-loop dynamics for pilot J}\right)$ with the system characteristics with the inner-loop dynamics changed to $\frac{0.5}{s^2}$ or $\frac{2}{s^2}$ but with the pilot's transfer function unchanged. Cases using both pitch and roll measured characteristics for pilot J and one case using measured roll characteristics for pilot D are presented. It can be seen that the short period oscillatory mode of motion changes from positive damping to negative damping in the tests in which the roll characteristics were used. For the case using pilot J pitch gains, the system did not go unstable.

Also shown in table III are the system characteristics of the inner loop alone with a substitution of K_3/s^2 dynamics. These results show that the inner loop alone does not go unstable following the damper failure. These results suggest that, should an unstable condition follow a damper failure in a multi-loop control task, a reasonable strategy would be to cease trying to control the outer loop and concentrate on the inner loop only. This exercise should continue until the pilot has become adjusted to the new dynamics. Then the pilot could return to controlling the multi-loop problem. The last entries

in tables III(a), (b), and (c) show the multi-loop system characteristics that can be expected after the pilot has become adapted to an inner-loop controlled element of K_3/s^2. These calculations show an improvement in the damping ratio of the attitude mode of motion, which becomes positive with pilot J but which remains slightly negative with pilot D.

Effect of control sensitivity changes in multi-loop control.- A qualitative investigation of the effect of control sensitivity changes in both the inner and outer loops on the control of the outer-loop variable was conducted. Engineer subjects were used. It was found that large changes could be made with little or no change occurring in the way in which the vehicle translation was controlled. A time history with the gains normally used in both inner and outer loop is shown in figure 15(a), and the effect of increasing the inner-loop control sensitivity by a factor of 10 is shown in figure 15(b). It can be seen that there is an increase in the frequency of the attitude mode of motion, but the translation mode of motion is unchanged. Figure 15(c) shows the result of leaving the inner-loop control sensitivity at normal setting and increasing the outer-loop sensitivity by a factor of 10. Once again the translation mode of motion is unchanged. The pilot still uses a limit on the attitude angle but this limit is reduced by a factor of 10 so that the limit value of translational acceleration is unchanged and, therefore, the translation maneuver is unchanged. Combining increases in both inner-loop and outer-loop sensitivity results in a small decrease in the time required to perform the translation maneuver, as is shown in figure 15(d).

The combination of a lower inner-loop sensitivity and a higher outer-loop sensitivity also results in a negligible change in performance. A maneuver done under these conditions is shown in figure 15(e). The higher outer-loop sensitivity compensates for the low inner-loop sensitivity. As long as the pilot is able to control the inner loop in a linear manner (or nearly linear manner), as is seen in figure 15(e), there is no change in the performance of the maneuver. However, when the sensitivity of the inner loop was greatly reduced and the sensitivity of the outer loop was not increased, a condition resulted in which the translation maneuver was greatly slowed down. (See figure 15(f).) The low sensitivity of the inner loop leads to a conflict between the pilot's desire for attitude control authority and the limit of this authority, which in the simulator was brought about by a limit in stick deflection. This conflict brought about a much slower control of the translation maneuver.

Extension of the multi-loop experiments.- The multi-loop experiments, again using the x,y plotter and dial display, were extended to determine the extreme combinations of visual feedback and vehicle dynamics which the human operator could control. It was found that the subjects could control a double-loop system with dynamics of $\frac{K_3}{s^2(s + 1)}$ in the inner loop. It has also been shown in references 9 and 10 that these dynamics contain the maximum controlled element lag with which a pilot can maintain stable control in a single-loop tracking task. A typical time history of the response of this double-loop system is shown in figure 16. The system was uncontrollable with a dynamics of K_3/s^3 in the inner loop.

It was also determined that the subjects could control a triple-loop system with dynamics of K_3/s^2 between each of the three visual feedbacks. In this case the three visual feedbacks were first, the dial; second, the horizontal displacement of the plotter; and third, the vertical displacement of the plotter. A block diagram of the system is shown in sketch (d). The displays were not meant to represent any particular vehicle motion but were presented to the subject as an abstract task. The subject's task was to change the vertical displacement of the plotter by a given distance. A typical run is shown in figure 17. If more controlled element lag was included in any of the three loops, such as putting $\frac{K_3}{s^2(s + 10)}$ dynamics in the inner loop, the system became uncontrollable.

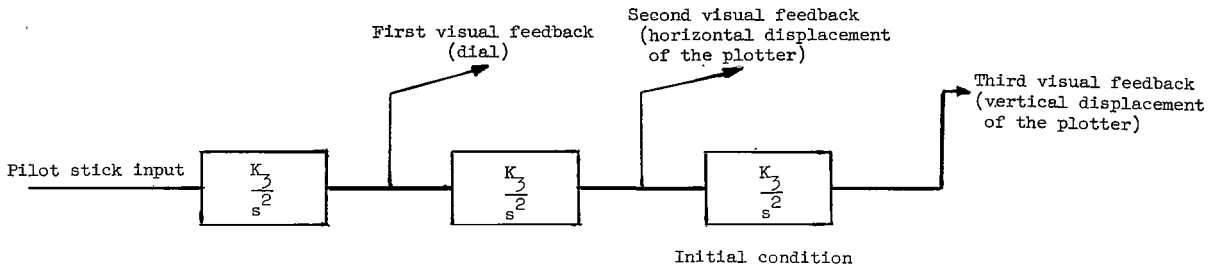

Sketch (d).- Block diagram of triple-loop simulation.

No attempt was made to reproduce these time histories using analog models for the pilot. It appears that with a system as complicated as the triple-loop system, that linear analog models, even linear models with output limits such as was used in the previous sections, will not suffice. Figure 17 shows that the pilot used what appears to be a preprogramed type of control strategy that is not linearly related to any of the displayed quantities.

It was also determined that these complex triple-loop systems were easier controlled with an on-off control than with the proportional control. Many of the records show that the pilot adapts to an on-off type of control output even when provided with a proportional controller. It is tentatively concluded that a proportional control offers no advantage in very complex and difficult to handle systems, and that the definite zero output position provided by on-off control is an advantage. The very definite dead band allows the pilot to take his attention away from the inner-loop display for short periods of time with the assurance that no inadvertent inputs will be made to the system.

Application of pilot transfer functions to a design problem.- The pilot transfer functions for the multi-loop lunar landing task developed in this investigation were used in making certain design calculations for a full-scale lunar landing simulator. Certain design compromises were required in the translation drive system of the simulator by the presence of high-frequency structural vibrations. Sample responses to step thrust inputs for three drive configurations are shown in figure 18(a).

Systems 1 and 2 are simplified systems, each with a different gain setting, and system 3 is a more elaborate system that uses additional control signal inputs. The system responses define the boundary of system performance that can be achieved in the presence of the structural vibration problem. It was felt that a proper decision on the suitability of these three systems could be made if a calculation of system response to an input similar to that expected with the pilot in the loop were made. Therefore, the design analysis was extended to include the multi-loop horizontal translation representation developed in the previous section, and the response both with and without the simulator drive dynamics was then determined. The results are shown in figure 18(b).

The response of the vehicle alone serves as a standard with which the three responses, which include the simulator drive dynamics, can be compared. The results show that the differences in the three systems do affect the manually controlled response and that system 1 gives a response that is more nearly like the ideal vehicle-alone response than does system 2. The apparent superiority of the alternate system, based on step input response, does not carry through to the manually controlled response, and therefore it was decided that the added mechanical complexity of the alternate system was not warranted. Therefore system 1 was recommended for use.

CONCLUSIONS

This investigation of human pilot transfer functions in multi-axis and multi-loop control systems supports the following conclusions:

1. A human pilot's response in multi-axis and double-loop control tasks can be well represented with linear constant-coefficient transfer functions.

2. Measurements made in multi-axis compensatory tracking tasks show that the pilot changes the response characteristics, and therefore the representative transfer function, so that the closed-loop system frequencies are reduced as the number of axes requiring control increases. It is shown that these results can be correlated with a theory that the pilot has a given maximum information processing capacity.

3. Two linear transfer functions, one for each loop, arranged in series are used to represent a pilot's response in a double-loop control task. Measured gains from multi-axis tracking tests can be used in the inner loop. The gains for the outer-loop pilot model are values that correspond to a system frequency much lower than those found in multi-axis tests. The gains for one particular control task are given in this paper.

4. These transfer functions can be used to give a quantitative description of system instabilities that result from unexpected vehicle dynamic changes

such as a damper failure. Also, the pilot transfer functions obtained from the multi-loop simulation can be used to provide useful design information.

Langley Research Center,
National Aeronautics and Space Administration,
Langley Station, Hampton, Va., October 15, 1965.

APPENDIX

CONVERSION OF U.S. CUSTOMARY UNITS TO SI UNITS

The International System of Units (SI) was adopted by the Eleventh General Conference on Weights and Measures, Paris, October 1960, in Resolution No. 12 (ref. 4). Conversion factors for the units used herein are as follows:

Length: $\begin{cases} \text{inches} \times 0.0254 = \text{meters} \quad (\text{m}) \\ \text{feet} \times 0.3048 = \text{meters} \quad (\text{m}) \end{cases}$

Acceleration: feet per second^2 $\times$ 0.3048 = meters per second^2 (m/sec^2)

Prefix to indicate multiple of unit: 10^{-2} centi (c)

REFERENCES

1. Adams, James J.; and Bergeron, Hugh P.: Measured Variation in the Transfer Function of a Human Pilot in Single-Axis Tasks. NASA TN D-1952, 1963.

2. Bergeron, Hugh P.; and Adams, James J.: Measured Transfer Functions of Pilots During Two-Axis Tasks With Motion. NASA TN D-2177, 1964.

3. Bergeron, Hugh P.; Kincaid, Joseph K.; and Adams, James J.: Measured Human Transfer Functions in Simulated Single-Degree-of-Freedom Nonlinear Control Systems. NASA TN D-2569, 1965.

4. Mechtly, E. A.: The International System of Units - Physical Constants and Conversion Factors. NASA SP-7012, 1964.

5. Shannon, C. E.: A Mathematical Theory of Communication. Bell System Tech. J., vol. XXVII, no. 3, July 1948, pp. 379-423.

6. Klemmer, Edmund T.: Discrete Tracking in One and Two Dimensions. AFCRC-TN-56-2, Air Force Cambridge Res. Center, Apr. 1956. (Also available as ASTIA AD No. 102689.)

7. Sadoff, Melvin: A Study of a Pilot's Ability to Control During Simulated Stability Augmentation System Failures. NASA TN D-1552, 1962.

8. Ashkenas, Irving L.; Jex, Henry R.; and McRuer, Duane T.: Pilot-Induced Oscillations: Their Cause and Analysis. Norair Rept. NOR-64-143 (Rept. STI TR-239-2), Northrop Corp., June 20, 1964.

9. Adams, James J.; Kincaid, Joseph K.; and Bergeron, Hugh P.: Determination of Critical Tracking Tasks for a Human Pilot. NASA TN D-3242, 1966.

10. Young, Laurence R.; and Meiry, Jacob L.: Bang-Bang Aspects of Manual Control in High Order Systems. M.I.T. paper presented at Joint Automatic Control Conference, Rensselaer Polytechnic Inst., June 22-25, 1965.

TABLE I.- SUMMARY OF DATA FOR MULTI-AXIS TESTS

(a) Pilot B

Dynamics, $\frac{2}{s(s + 1)}$

Axis	Disturbance break point frequency, rad/sec	Measured gains			Closed-loop characteristics			Root-mean-square error, volts	Normalized error
					Oscillatory		Real roots		
		K_1	τ	K_2	ω_n, rad/sec	ζ			
Y_1	0.25	37	10	3.5	3.34	0.34	-4.75, -14.0	0.82	0.090
Y_2	.25	18	7	4	3.31	.36	-2.21, -10.4	1.28	.140
Y_3	.06	7.5	7	5	2.20	.69	-2.24, -9.71	1.34	[a].298
X_1	.25	33	7.5	2.5	3.55	.10	-3.27, -12.0	1.88	.206
X_2	.25	31	7.5	2.5	3.29	.18	-3.95, -10.8	2.4	.263
X_3	.06	10	6.5	5	3.02	.47	-1.48, -9.66	1.34	[a].298
Z_1	.25	12	3.5	3.5	3.47	.004	-1.00, -6.97	.907	.099
Z_3	.06	7	3.5	1.5	1.94	.08	-2.51, -5.16	1.0	[a].222

[a]From the estimated value of the disturbance root mean square.

TABLE I.- SUMMARY OF DATA FOR MULTI-AXIS TESTS - Continued

(b) Pilot D

Dynamics, $\frac{0.5}{s(s + 0.5)}$; disturbance break point frequency, 0.125 rad/sec

Axis	Measured gains			Closed-loop characteristics			Root-mean-square error, volts	Normalized error
				Oscillatory		Real roots		
	K_1	τ	K_2	ω_n, rad/sec	ζ			
Y_1	11	3.8	8.5	2.70	0.21	-0.44, -6.49	0.40	0.065
Y_2	15.5	5.5	4.0	1.41	.42	-2.89, -7.41	.58	.095
Y_3	15	7.5	3.8	1.05	.37	-5.68, -9.03	1.17	.192
X_1	25	7.5	6.5	1.74	.64	-3.03, -10.23	.64	.105
X_2	16	6.0	2.5	1.20	.26	-4.47, -7.40	1.15	.189
X_3	16	7.5	3.3	1.07	.34	-5.83, -8.94	1.60	.262
Z_1	12.5	6.0	5.8	1.27	.62	-2.87, -8.05	.84	.138
Z_3	5.0	10.5	3.0	.47	.53	-9.36, -11.6	1.84	.302
Dynamics, $\frac{0.5}{s^2}$								
Y_2	9.5	7.5	8.2	0.87	0.34	-4.97, -9.43	0.63	0.103
Y_3	7.0	7.0	8.5	.77	.34	-4.72, -8.75	1.54	.252
X_2	7.0	8.5	8.0	.67	.23	-6.62, -10.1	1.77	.290
X_3	5.0	11	10.2	.48	.18	-9.45, -12.4	3.46	.568
Z_3	3.2	9.0	10.6	1.58	.08	-1.31, -4.83	6.24	1.02

TABLE I.- SUMMARY OF DATA FOR MULTI-AXIS TESTS - Continued

(c) Pilot J

Dynamics, $\frac{2}{s(s+1)}$; disturbance break point frequency, 0.25 rad/sec

Axis	Measured gains			Closed-loop characteristics			Root-mean-square error, volts	Normalized error
				Oscillatory		Real roots		
	K_1	τ	K_2	ω_n, rad/sec	ζ			
Y_1	12	6.0	6.0	3.83	0.28	-1.0, -9.83	0.99	0.108
Y_2	8.0	6.5	6.5	3.26	.50	-1.0, -9.76	1.22	.133
Y_3	6.0	5.0	5.8	3.02	.36	-0.83, -7.98	1.41	.154
X_1	7.0	6.5	4.5	2.11	.63	-2.25, -9.06	1.62	.177
X_2	5.0	5.0	3.0	1.72	.47	-2.43, -6.96	2.39	.262
X_3	3.0	5.5	5.0	1.71	.88	-1.5, -7.49	2.80	.306
Z_1	6.0	5.0	3.0	1.93	.42	-2.26, -7.12	1.31	.143
Z_3	3.5	3.5	2.5	1.71	.34	-1.60, -5.24	2.27	.249
Dynamics, $\frac{2}{s^2}$								
Y_1	8.0	7.0	9.5	3.32	0.36	-0.96, -10.6	1.16	0.127
Y_2	8.5	7.5	7.5	2.52	.47	-1.87, -10.8	1.89	.206
Y_3	6.0	8.0	10	2.07	.68	-2.0, -11.1	2.5	.274
X_2	5.0	7.0	5.0	1.35	.25	-4.18, -9.15	3.41	.383
X_3	5.0	7.5	5.0	1.27	.23	-4.83, -9.6	3.42	.384
Z_3	5.5	7.0	7.5	1.24	.35	-5.60, -11.5	3.74	.410

TABLE I.- SUMMARY OF DATA FOR MULTI-AXIS TESTS - Concluded

(d) Pilot L

Dynamics, $\frac{0.5}{s(s + 0.5)}$, disturbance break point frequency = 0.125 rad/sec

Axis	Measured gains			Closed-loop characteristics			Root-mean-square error, volts	Normalized error
				Oscillatory		Real roots		
	K_1	τ	K_2	ω_n, rad/sec	ζ			
Y_1	7.5	4.0	5.5	1.70	0.52	-0.89, -5.84	0.53	0.087
Y_2	9.4	4.8	5.0	1.32	.59	-1.97, -6.57	.69	.113
Y_3	8.0	5.0	5.3	1.12	.62	-2.40, -6.71	.81	.133
X_1	7.5	4.8	7.8	1.94	.67	-0.70, -6.81	.56	.092
X_2	11.5	4.5	2.6	1.22	.28	-3.02, -5.80	1.17	.192
X_3	11.0	7.5	5.0	1.06	.37	-5.43, -9.29	2.5	.41
Z_1	8.0	3.7	4.0	1.43	.38	-1.47, -5.32	.58	.095
Z_3	6.0	5.0	7.4	1.20	.91	-1.53, -6.78	1.12	.183

TABLE II.- RATIO OF SYSTEM NATURAL FREQUENCIES

FOR DIFFERENT MULTI-AXIS TESTS

Dynamics, $\frac{0.5}{s(s + 0.5)}$ or $\frac{2}{s(s + 1)}$

Ratio	Pilot B	Pilot D	Pilot J	Pilot L	Average
Y_2/Y_1	0.99	0.52	0.85	0.77	0.78
X_2/X_1	.92	.69	.81	.63	.76
Y_3/Y_1	0.66	0.39	0.79	0.66	0.63
X_3/X_1	.85	.62	.81	.55	.70
Z_3/Z_1	.55	.38	.88	.83	.66
Y_3/Y_2	0.67	0.75	0.93	0.86	0.80
X_3/X_2	.93	.90	1.0	.87	.93
Dynamics, $\frac{0.5}{s^2}$ or $\frac{2}{s^2}$					
Y_2/Y_1	----	----	0.76	----	0.76
Y_3/Y_1	----	----	0.62	----	0.62
X_3/X_2	----	0.74	0.94	----	0.84
Y_3/Y_2	----	.88	.85	----	.87

TABLE III.- CLOSED-LOOP CHARACTERISTICS FOR MULTI-LOOP SYSTEMS

(a) Pilot D, using measured pilot gains for X_2 run

Measured gains						Controlled elements		Characteristics		
Inner loop			Outer loop			Inner loop	Outer loop	ω_n, rad/sec	ζ	Real roots
K_1	τ	K_2	K_1	τ	K_2					
						Inner loop				
16	6	2.5				$\frac{0.5}{s(s + 0.5)}$		1.20	0.26	-4.47 -7.40
						Outer loop				
			0.09	10	92		$\frac{5.36}{s^2}$	------	------	-0.176 -.302 -7.60 -11.9
						Complete system				
16	6	2.5	0.09	10	92	$\frac{0.5}{s(s + 0.5)}$	$\frac{5.36}{s^2}$	1.11 10.2	0.046 .99	-0.167 -.336 -4.75 -6.85
						Complete system				
16	6	2.5	0.09	10	92	$\frac{0.5}{s^2}$	$\frac{5.36}{s^2}$	1.20 10.1	-0.15 .99	-0.185 -.256 -4.82 -6.83
						Inner loop				
16	6	2.5				$\frac{0.5}{s^2}$		1.20	0.037	-4.56 -7.35
						Complete system				
7.0	8.5	8.0	0.09	10	92	$\frac{0.5}{s^2}$	$\frac{5.36}{s^2}$	0.737 .197 7.57 10.8	-0.094 .98 .99 .99	-------

TABLE III.- CLOSED-LOOP CHARACTERISTICS FOR MULTI-LOOP SYSTEMS - Continued

(b) Pilot J, using measured pilot gains for X_2 run

Measured gains						Controlled elements		Characteristics		
Inner loop			Outer loop			Inner loop	Outer loop	ω_n, rad/sec	ζ	Real roots
K_1	τ	K_2	K_1	τ	K_2					
Inner loop										
5.0	5.0	3.0				$\frac{2}{s(s+1)}$		1.72	0.47	-2.43 -6.96
Outer loop										
			0.09	10	92		$\frac{5.36}{s^2}$	-----	------	-0.176 -.302 -7.60 -11.9
Complete system										
5.0	5.0	3.0	0.09	10	92	$\frac{2}{s(s+1)}$	$\frac{5.36}{s^2}$	1.40 10.2	0.33 .99	-0.162 -.410 -2.82 -6.40
Complete system										
5.0	5.0	3.0	0.09	10	92	$\frac{2}{s^2}$	$\frac{5.36}{s^2}$	1.54 10.2	-0.077 .99	-0.181 -.269 -3.21 -6.31
Inner loop										
5.0	5.0	3.0				$\frac{2}{s^2}$		1.59	0.086	-2.90 -6.82
Complete system										
5.0	7.0	5.0	0.09	10	92	$\frac{2}{s^2}$	$\frac{5.36}{s^2}$	1.33 10.6	0.029 .99	-0.185 -.255 -4.77 -7.53

TABLE III.- CLOSED-LOOP CHARACTERISTICS FOR MULTI-LOOP SYSTEMS - Concluded

(c) Pilot J, using measured pilot gains for Y_2 run

Measured gains						Controlled elements		Characteristics		
Inner loop			Outer loop			Inner loop	Outer loop	ω_n, rad/sec	ζ	Real roots
K_1	τ	K_2	K_1	τ	K_2					
Inner loop										
8.0	6.5	6.5				$\frac{2}{s(s+1)}$		3.26	0.50	-1.0 -9.76
Outer loop										
			0.09	10	92		$\frac{5.36}{s^2}$	-----	-----	-0.176 -.302 -7.60 -11.9
Complete system										
8.0	6.5	6.5	0.09	10	92	$\frac{2}{s(s+1)}$	$\frac{5.36}{s^2}$	2.84 11.0	0.55 .99	-0.163 -.423 -1.00 -7.49
Complete system										
8.0	6.5	6.5	0.09	10	92	$\frac{2}{s^2}$	$\frac{5.36}{s^2}$	2.24 10.9	0.24 .99	-0.181 -.270 -2.30 -7.48
Inner loop										
8.0	6.5	6.5				$\frac{2}{s^2}$		2.61	0.345	-1.58 -9.61
Complete system										
8.5	7.5	7.5	0.09	10	92	$\frac{2}{s^2}$	$\frac{5.36}{s^2}$	2.06 11.4	0.32 .99	-0.181 -.267 -3.03 -7.60

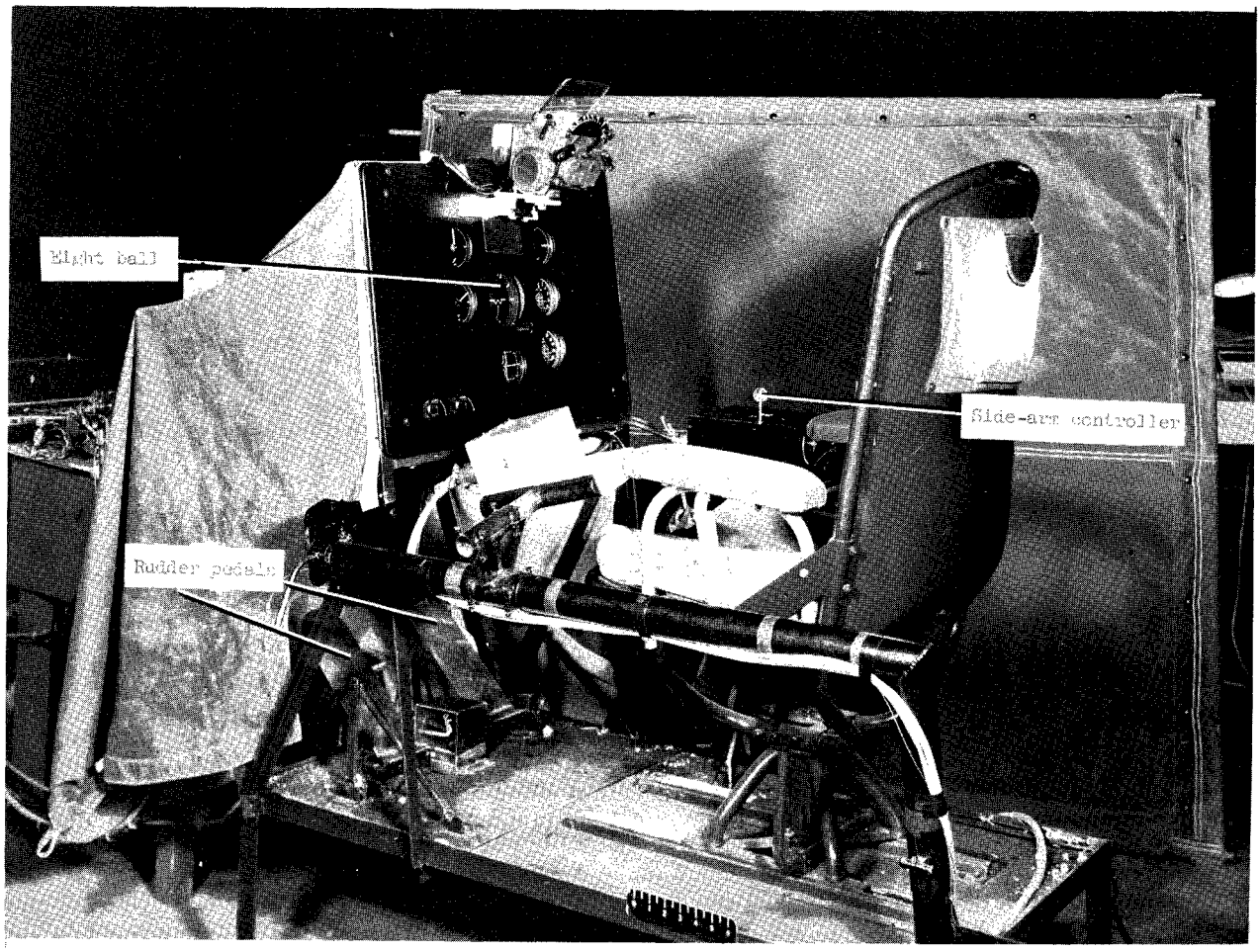

Figure 1.- Photograph of fixed-base multi-axis simulator. L-61-2652.1

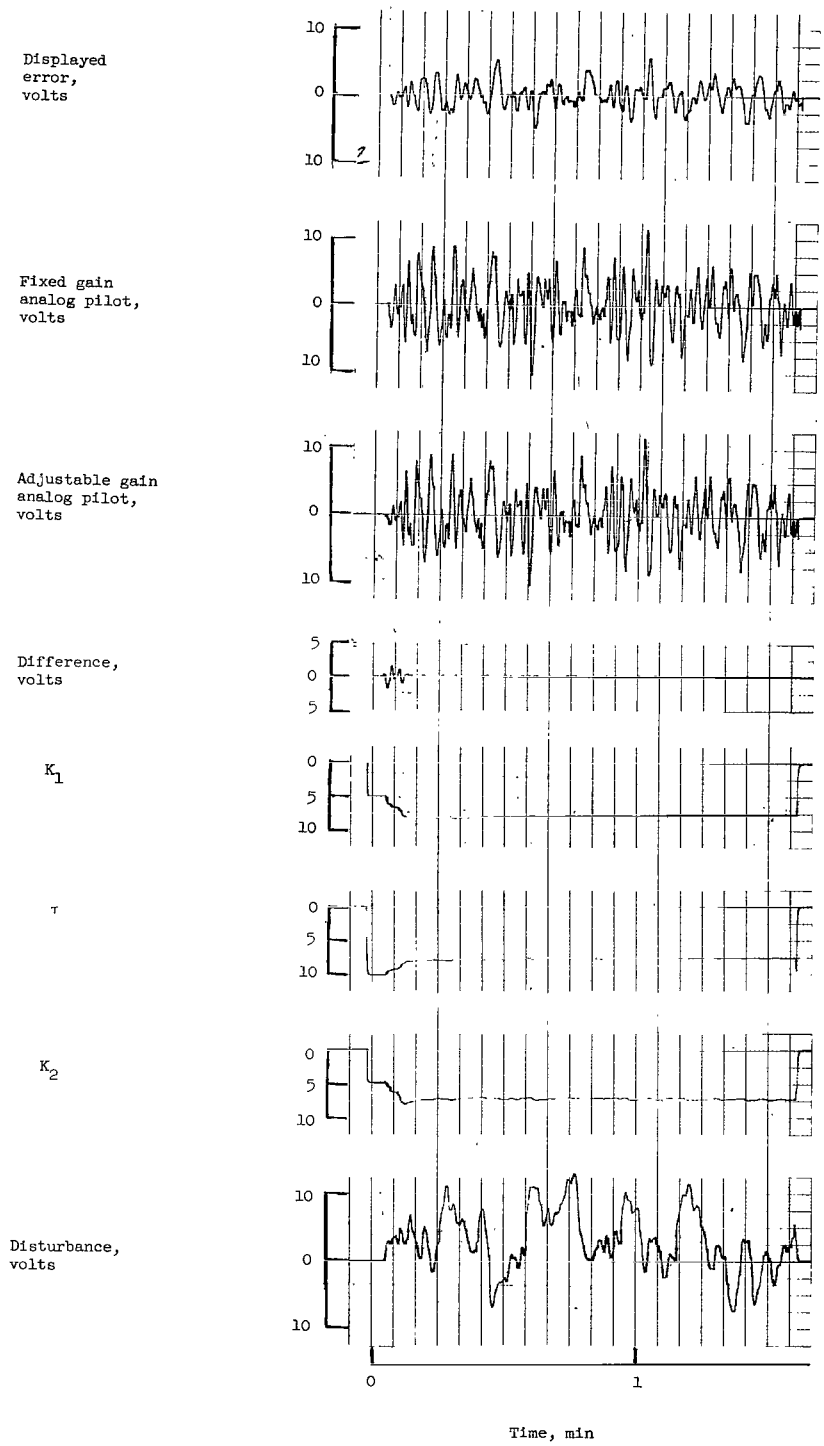

Figure 2.- Gain adjustment to a known fixed gain model.

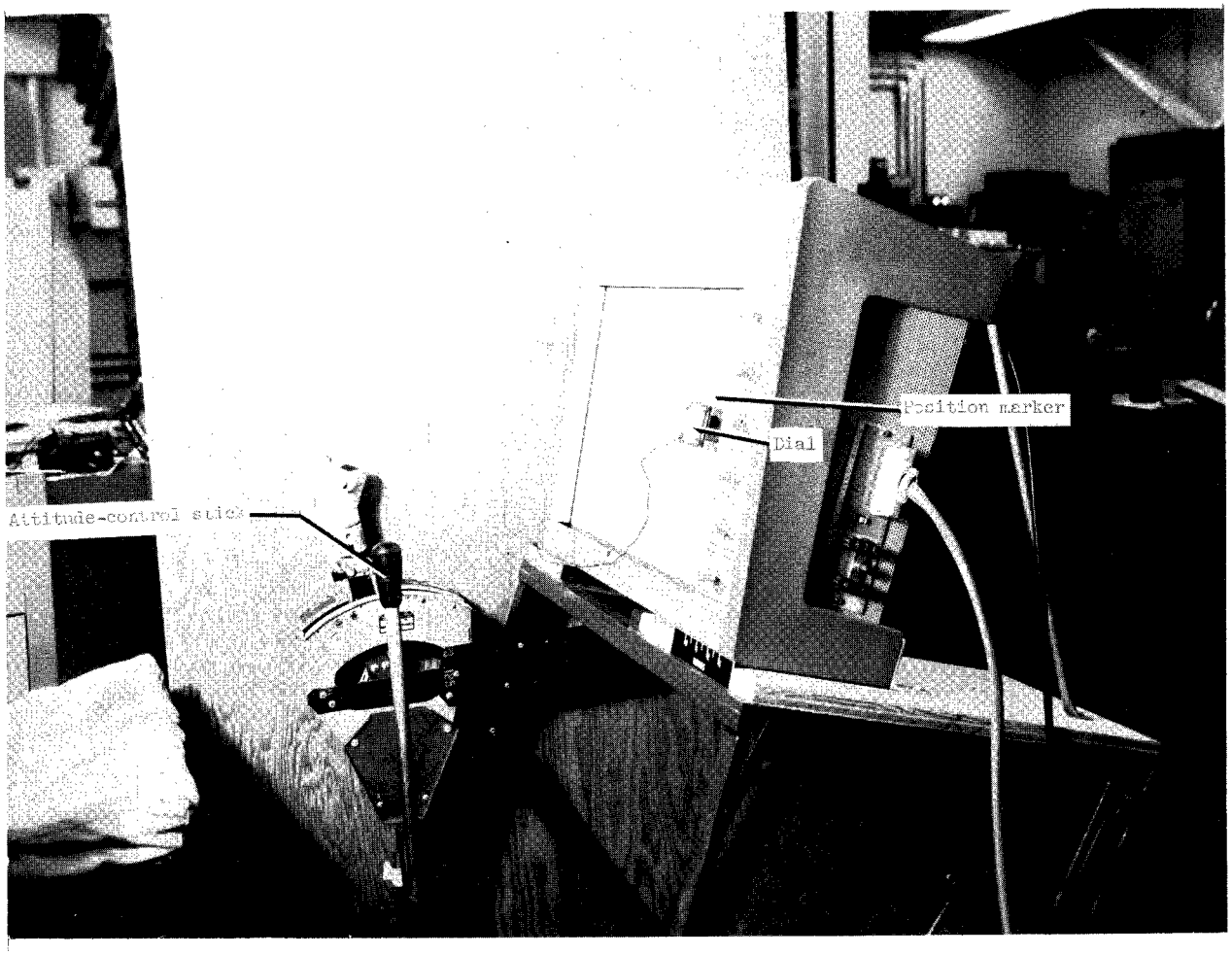

Figure 3.- Photograph of x,y plotter used in multi-axis simulation. L-62-4272.1

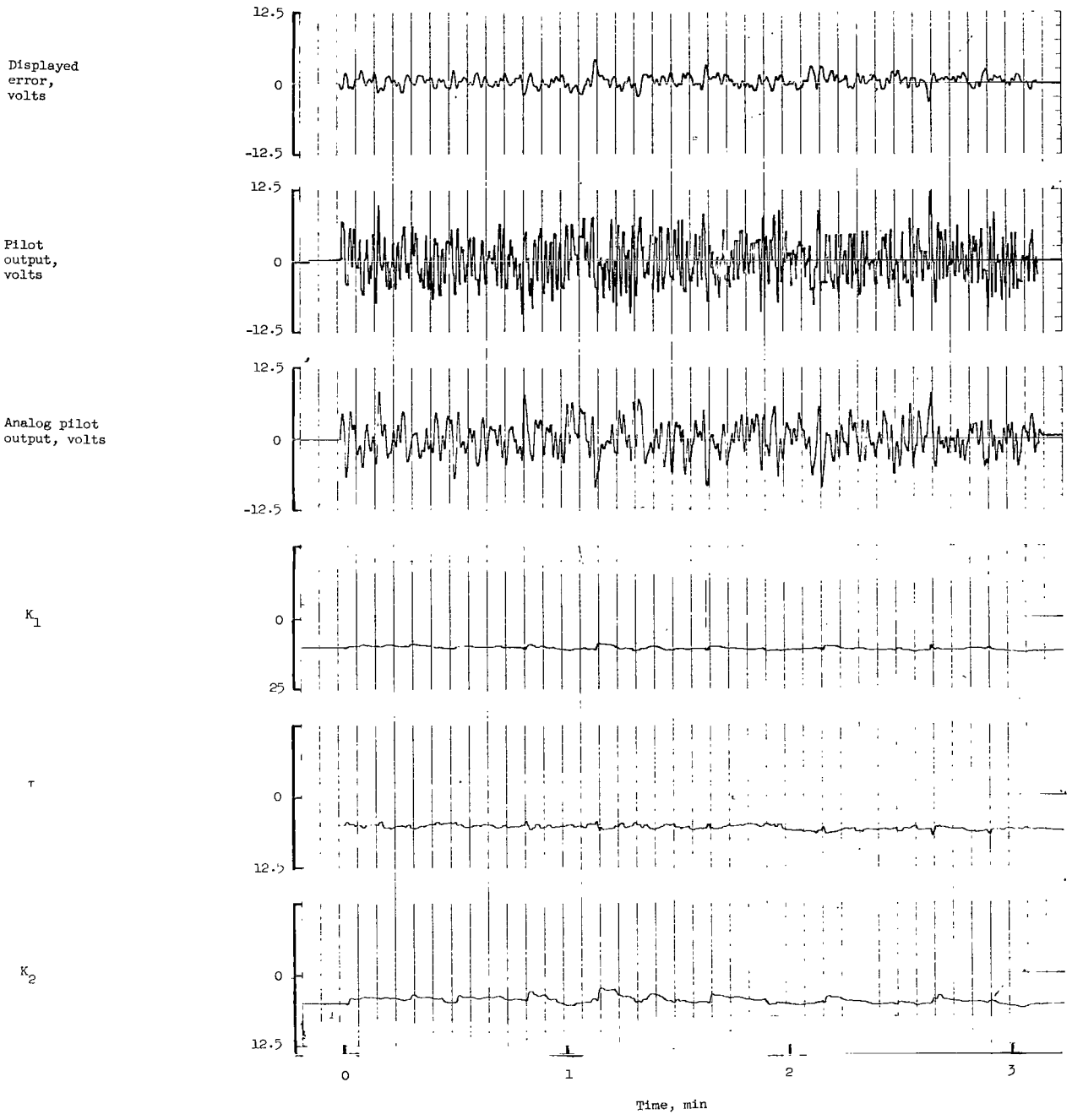

Figure 4.- Record of pilot J with dynamics of $\frac{2}{s(s+1)}$. Pitch axis of a single-axis run.

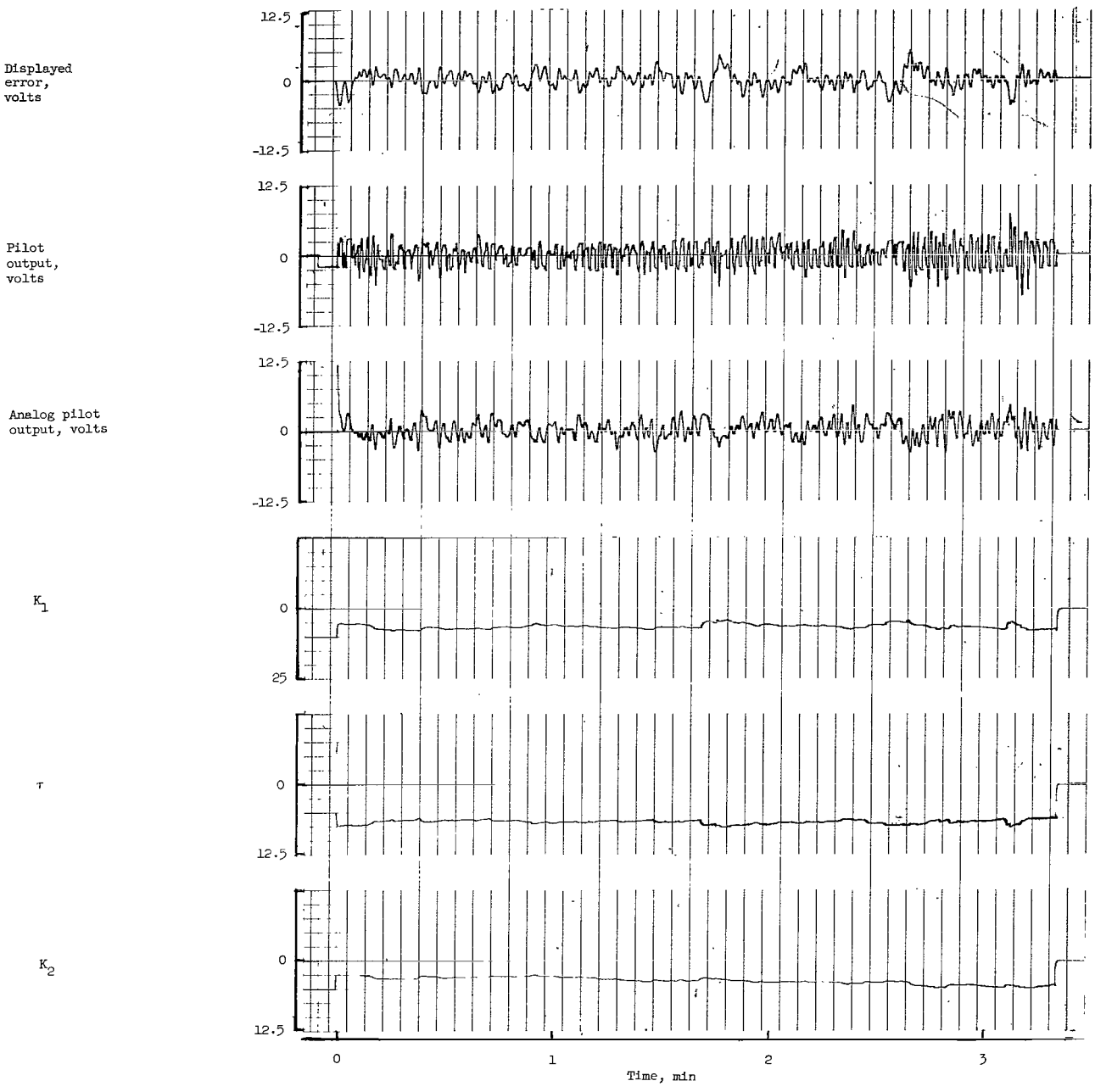

Figure 5.- Record of pilot J with dynamics of $\frac{2}{s(s + 1)}$. Roll axis of a single-axis run.

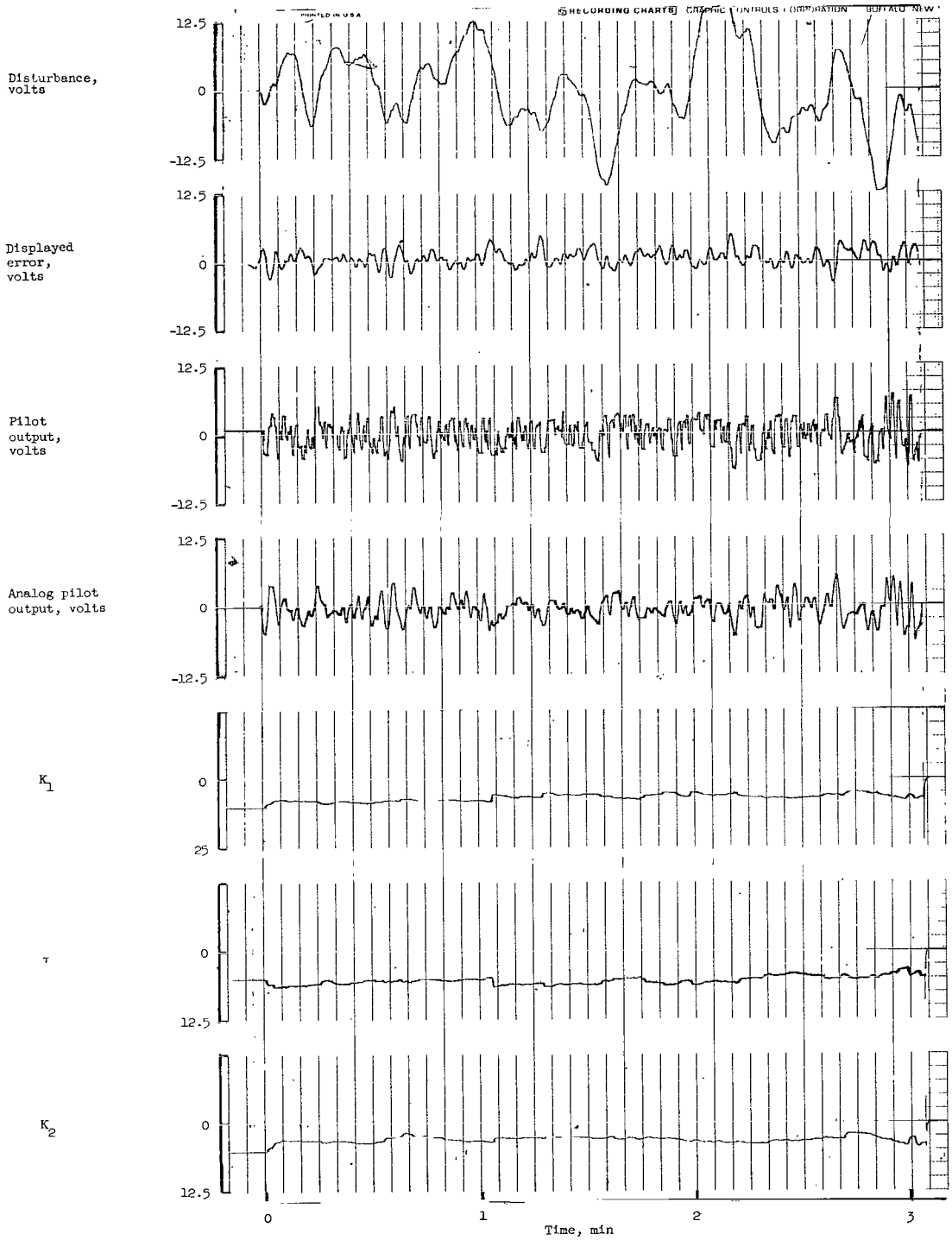

Figure 6.- Record of pilot J with dynamics of $\frac{2}{s(s + 1)}$. Yaw axis of a single-axis run.

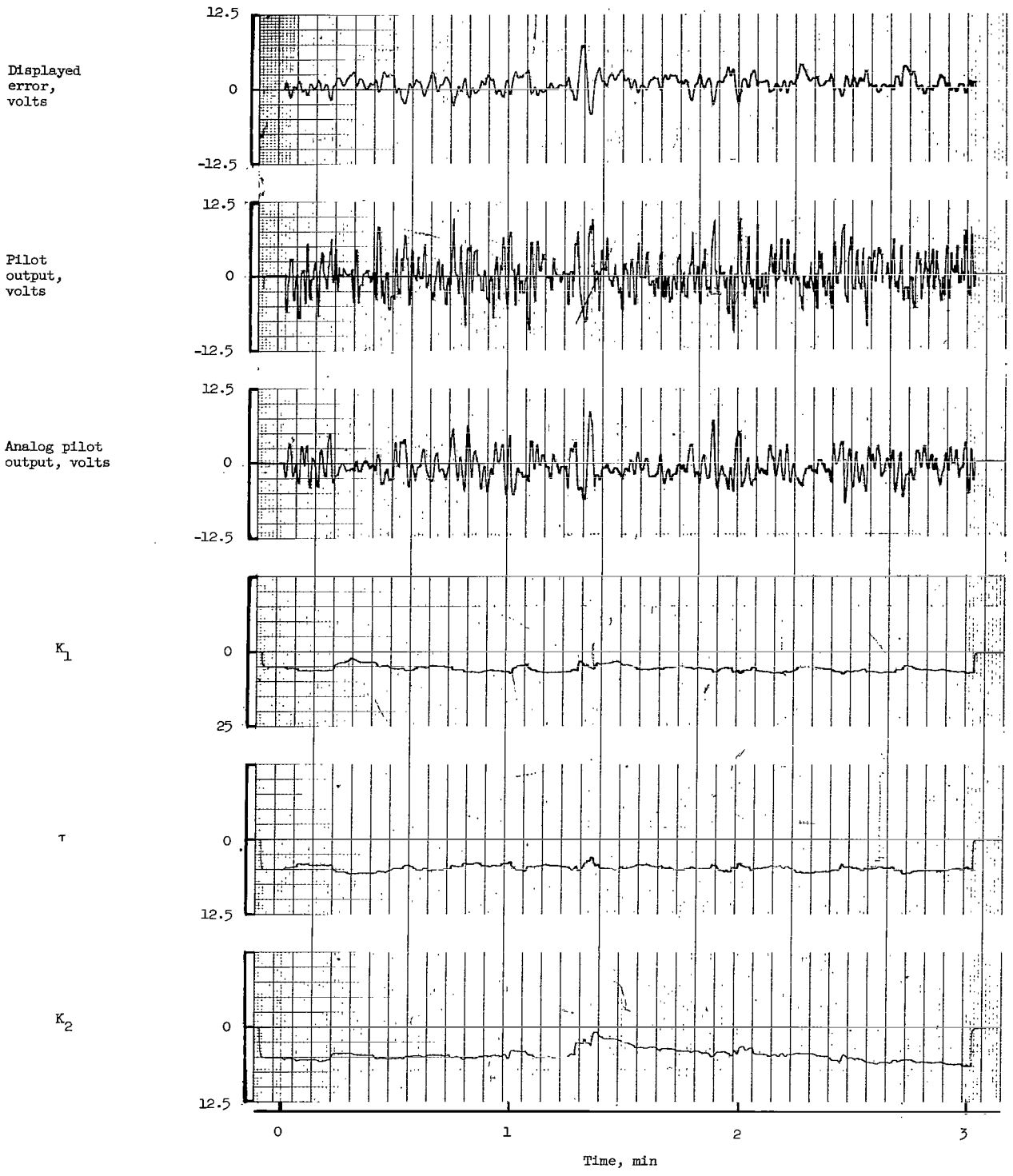

Figure 7.- Record of pilot J with dynamics of $\frac{2}{s(s+1)}$. Pitch axis of a three-axis run.

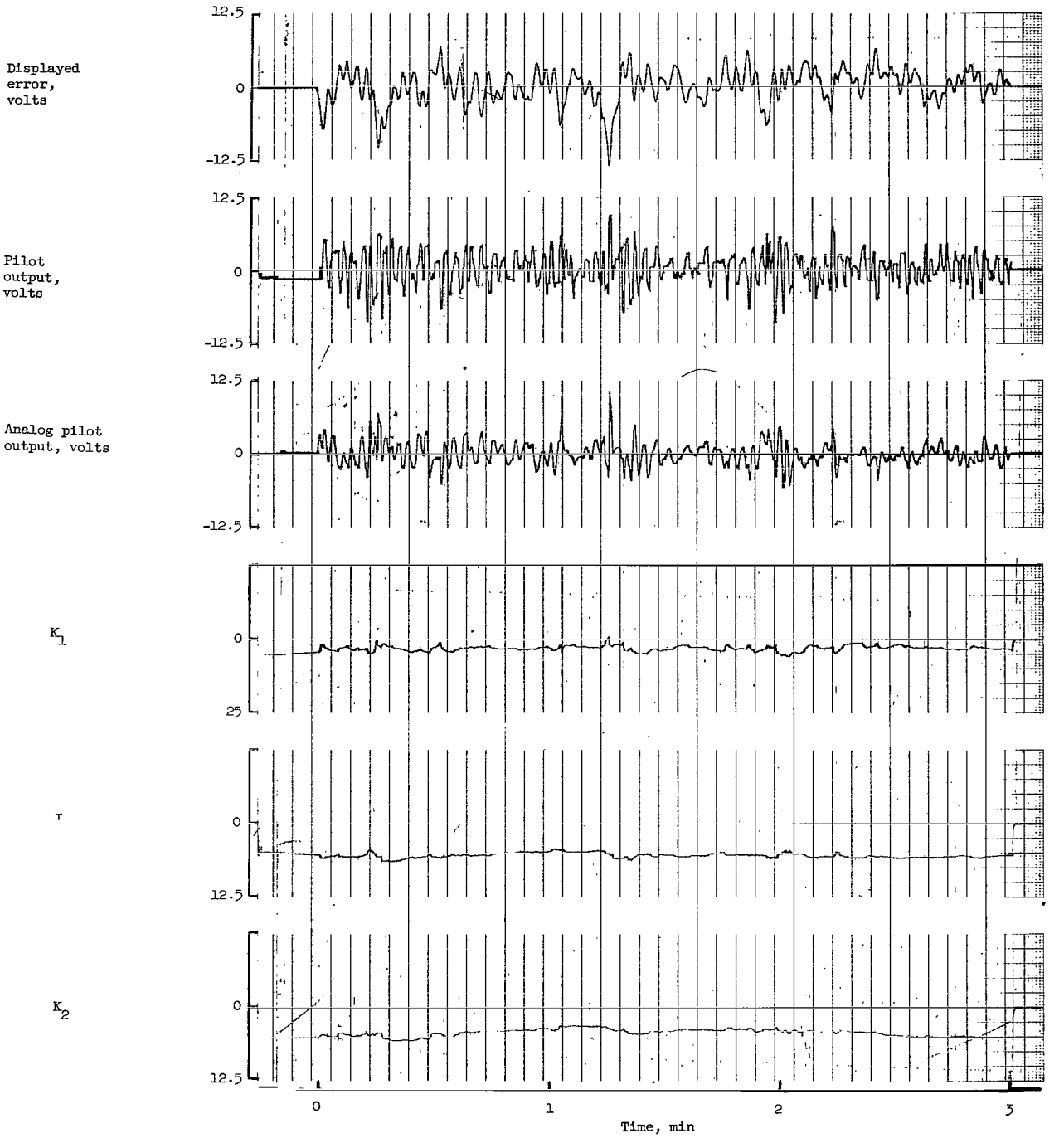

Figure 8.- Record of pilot J with dynamics of $\frac{2}{s(s + 1)}$. Roll axis of a three-axis run.

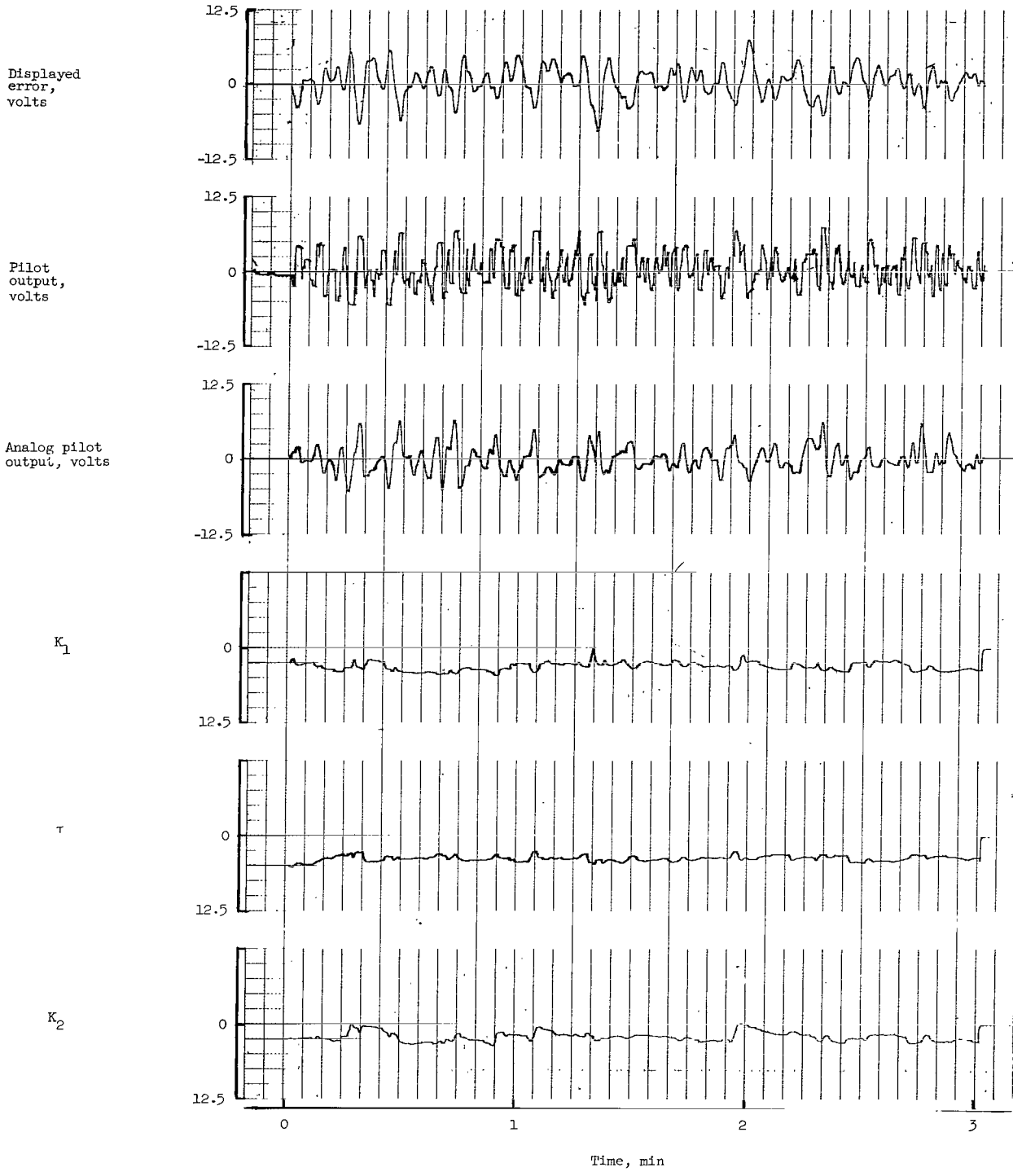

Figure 9.- Record of pilot J with dynamics of $\frac{2}{s(s + 1)}$. Yaw axis of a three-axis run.

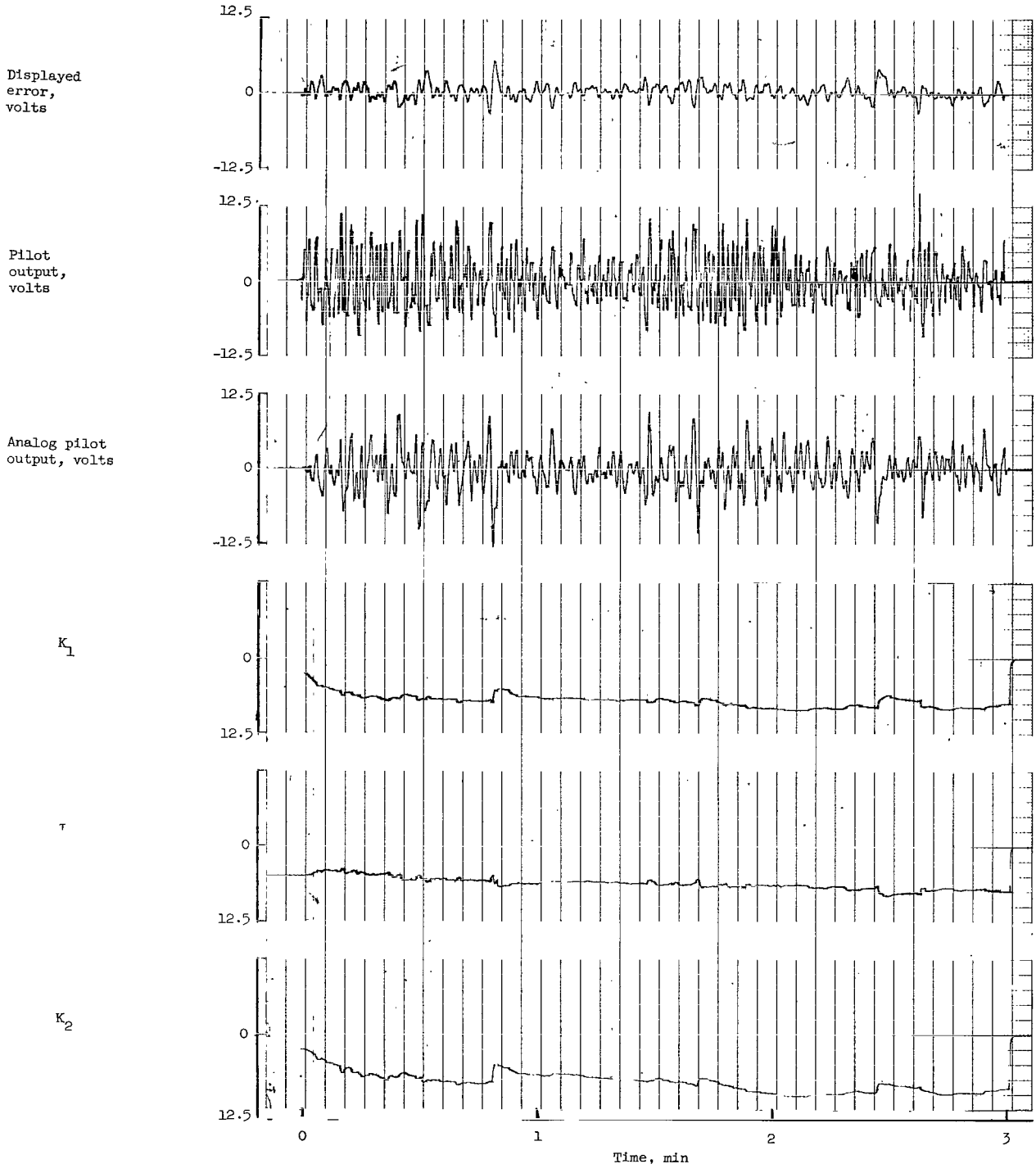

Figure 10.- Record of pilot J with dynamics of $\frac{2}{s^2}$. Pitch axis of a single-axis run.

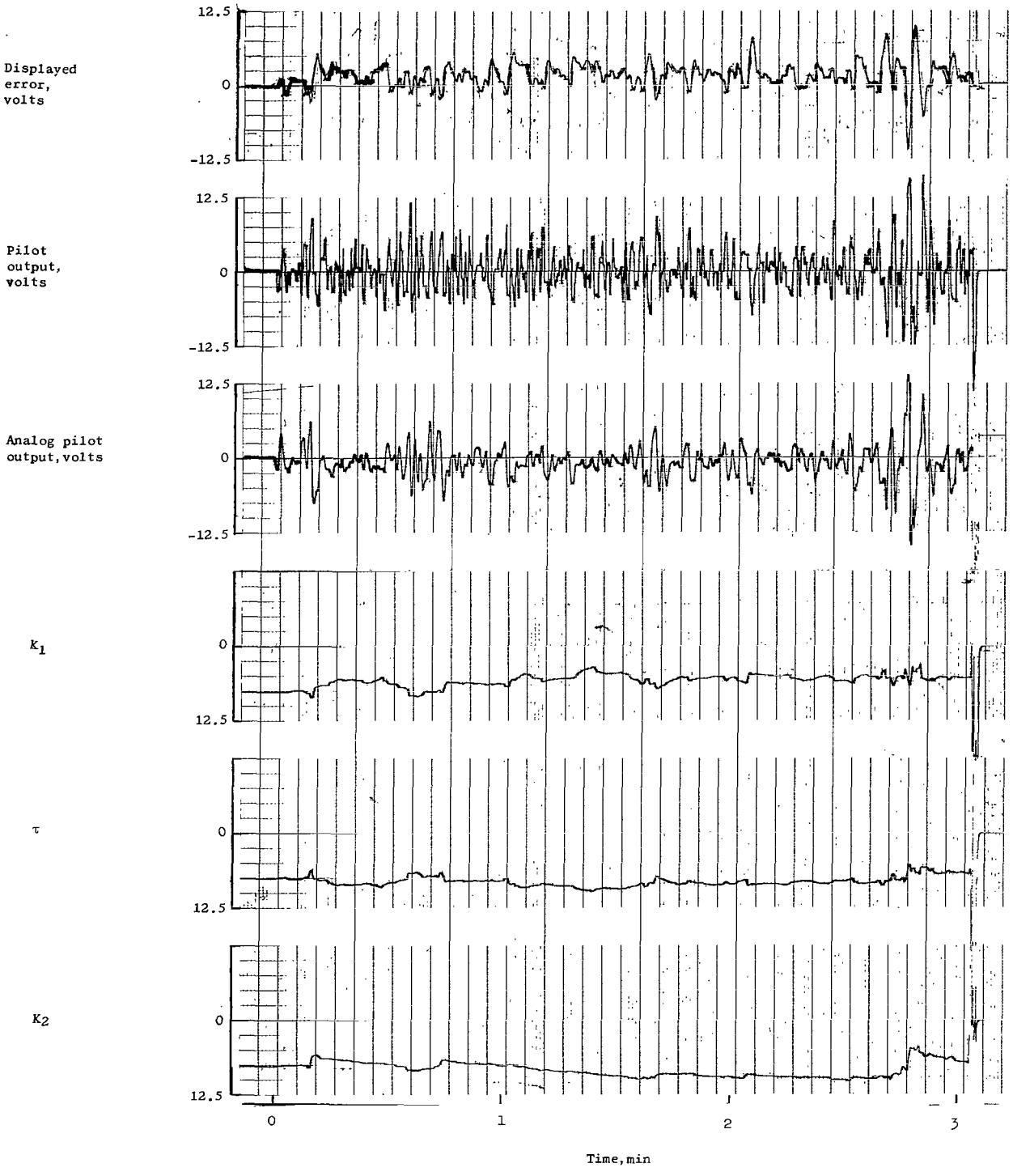

Figure 11.- Record of pilot J with dynamics of $\frac{2}{s^2}$. Pitch axis of a three-axis run.

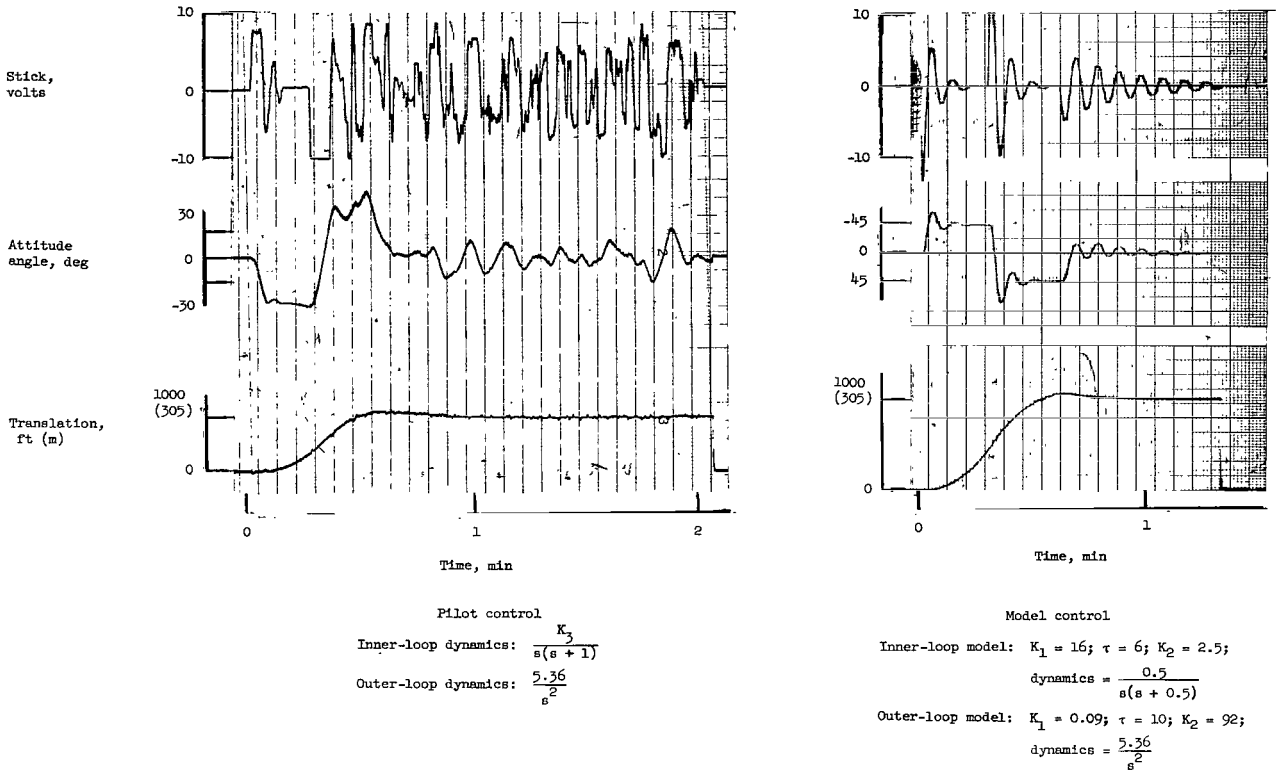

Pilot control

Inner-loop dynamics: $\frac{K_3}{s(s+1)}$

Outer-loop dynamics: $\frac{5.36}{s^2}$

Model control

Inner-loop model: $K_1 = 16$; $\tau = 6$; $K_2 = 2.5$;

dynamics = $\frac{0.5}{s(s+0.5)}$

Outer-loop model: $K_1 = 0.09$; $\tau = 10$; $K_2 = 92$;

dynamics = $\frac{5.36}{s^2}$

Figure 12.- Comparison of pilot and model in a multi-loop simulation.

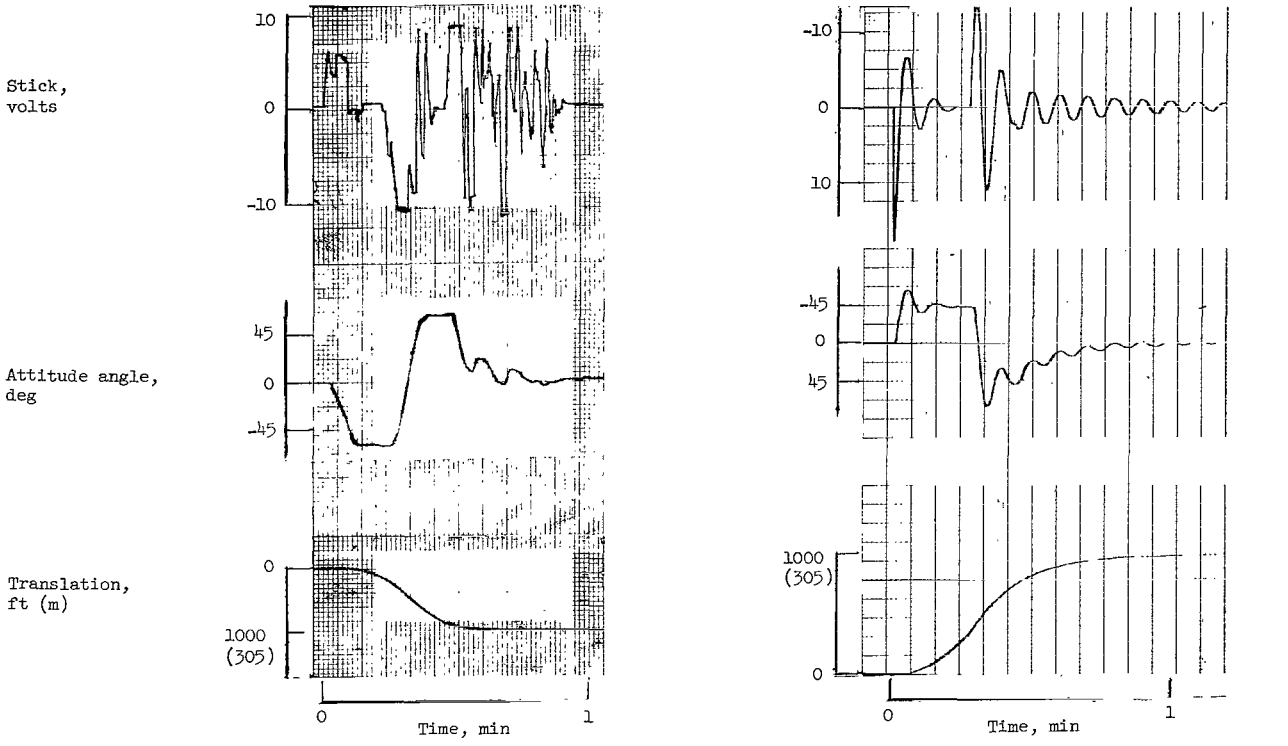

Figure 13.- Comparison of pilot and model in a multi-loop simulation.

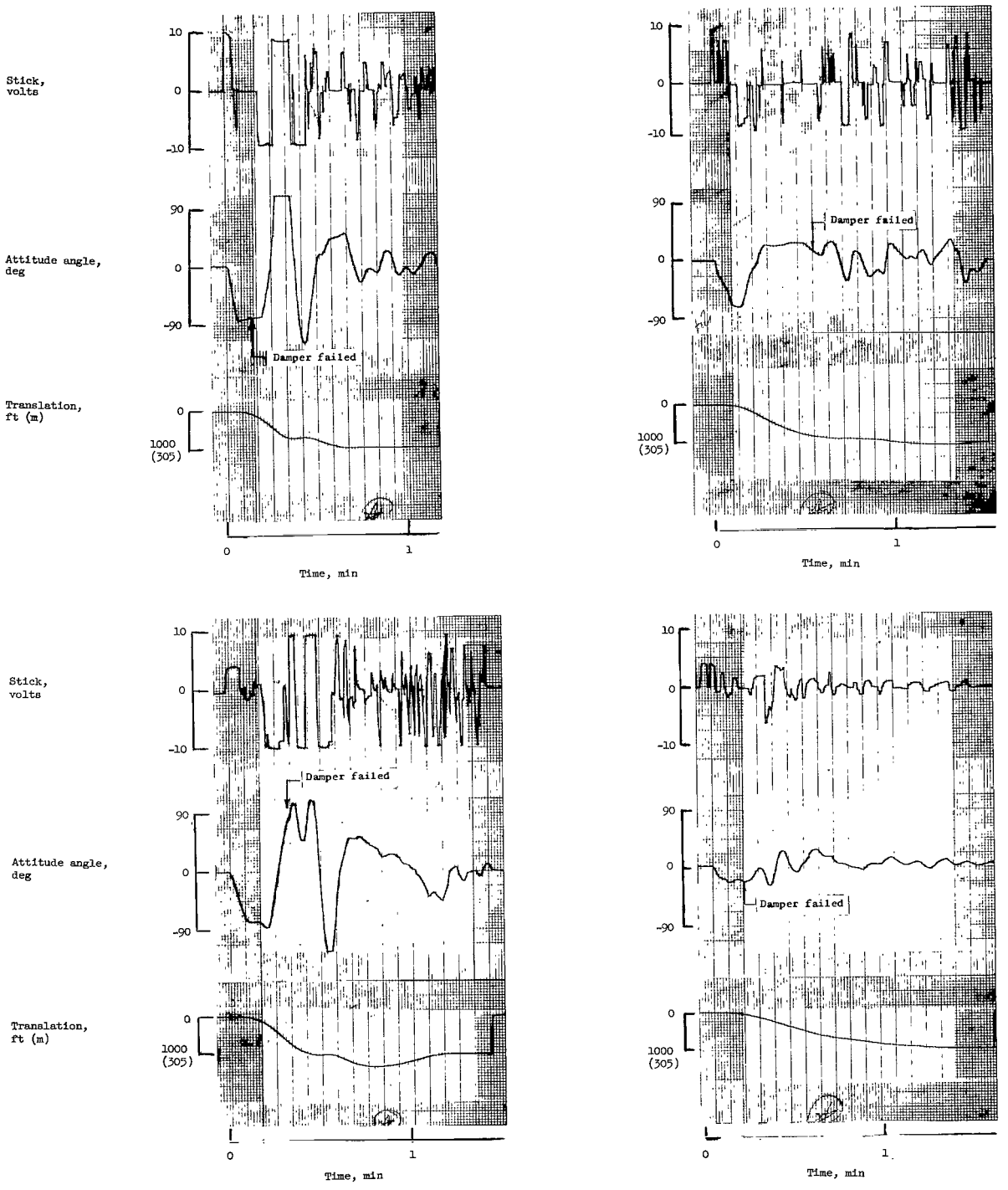

Figure 14.- Multi-loop runs with unexpected damper failures (as noted by arrows).

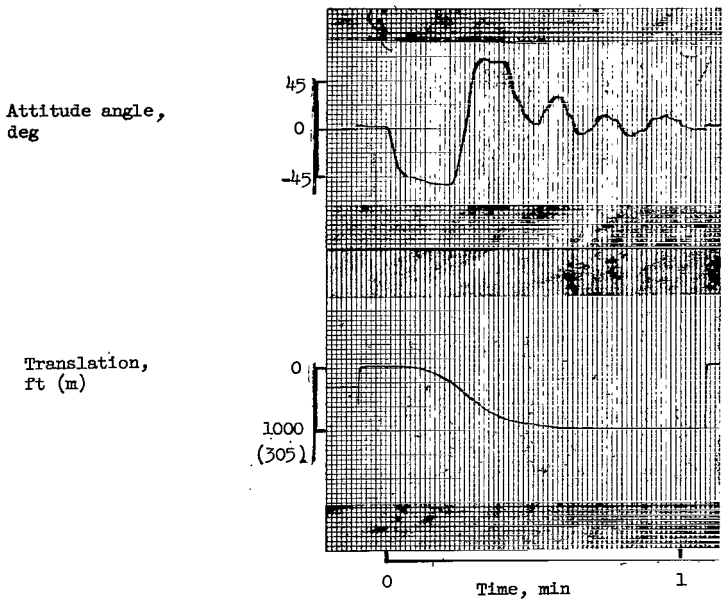

(a) Control sensitivity, normal.

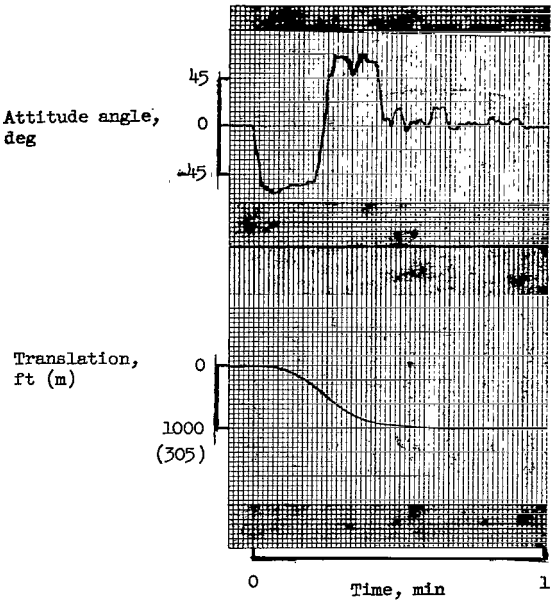

(b) Inner-loop sensitivity, 10 × normal; outer-loop sensitivity, normal.

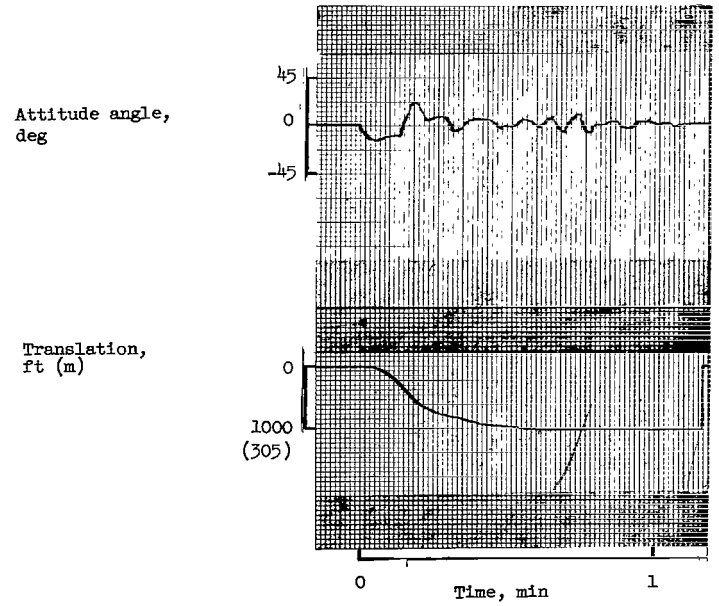

(c) Inner-loop sensitivity, normal; outer-loop sensitivity, 10 × normal.

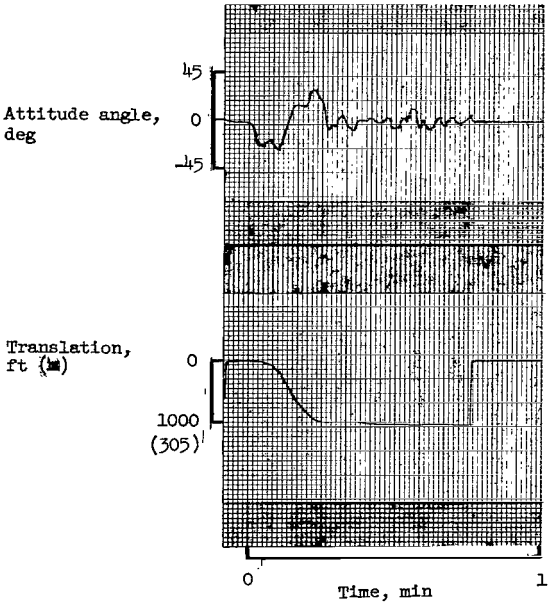

(d) Inner-loop sensitivity, 10 × normal; outer-loop sensitivity, 10 × normal.

Figure 15.- Control sensitivity experiments.

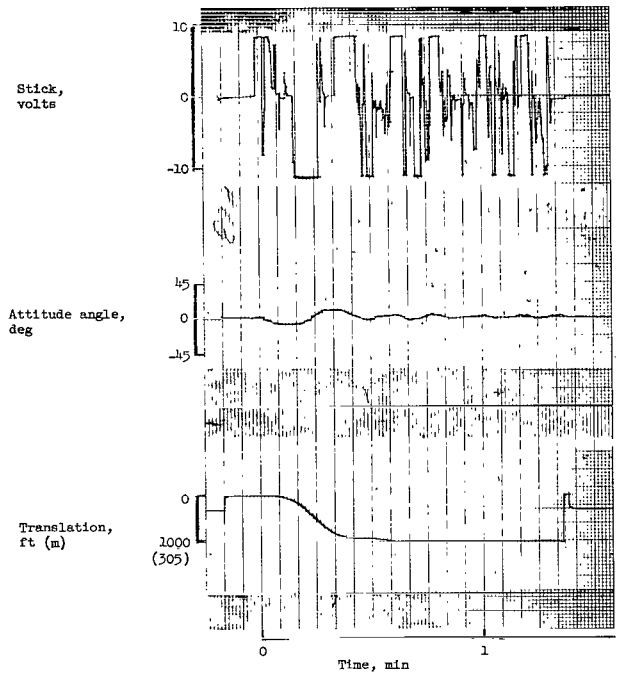

(e) Inner-loop sensitivity, 0.1 × normal; outer-loop sensitivity, 10 × normal.

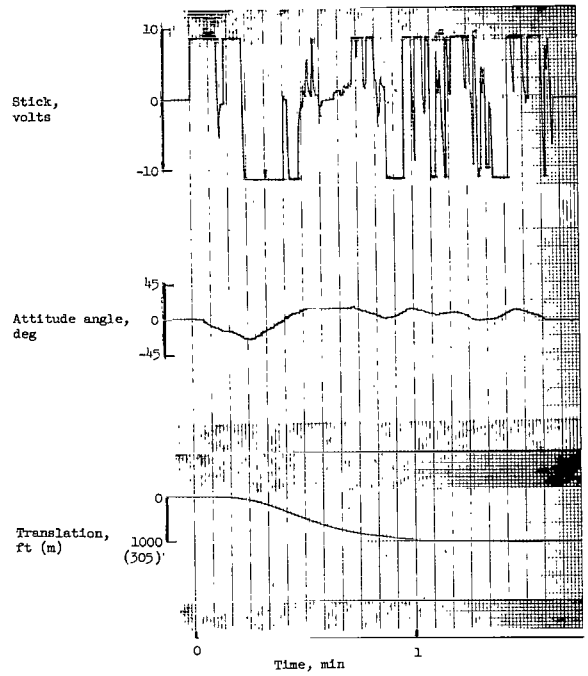

(f) Inner-loop sensitivity, 0.1 × normal; outer-loop sensitivity, normal.

Figure 15.- Concluded.

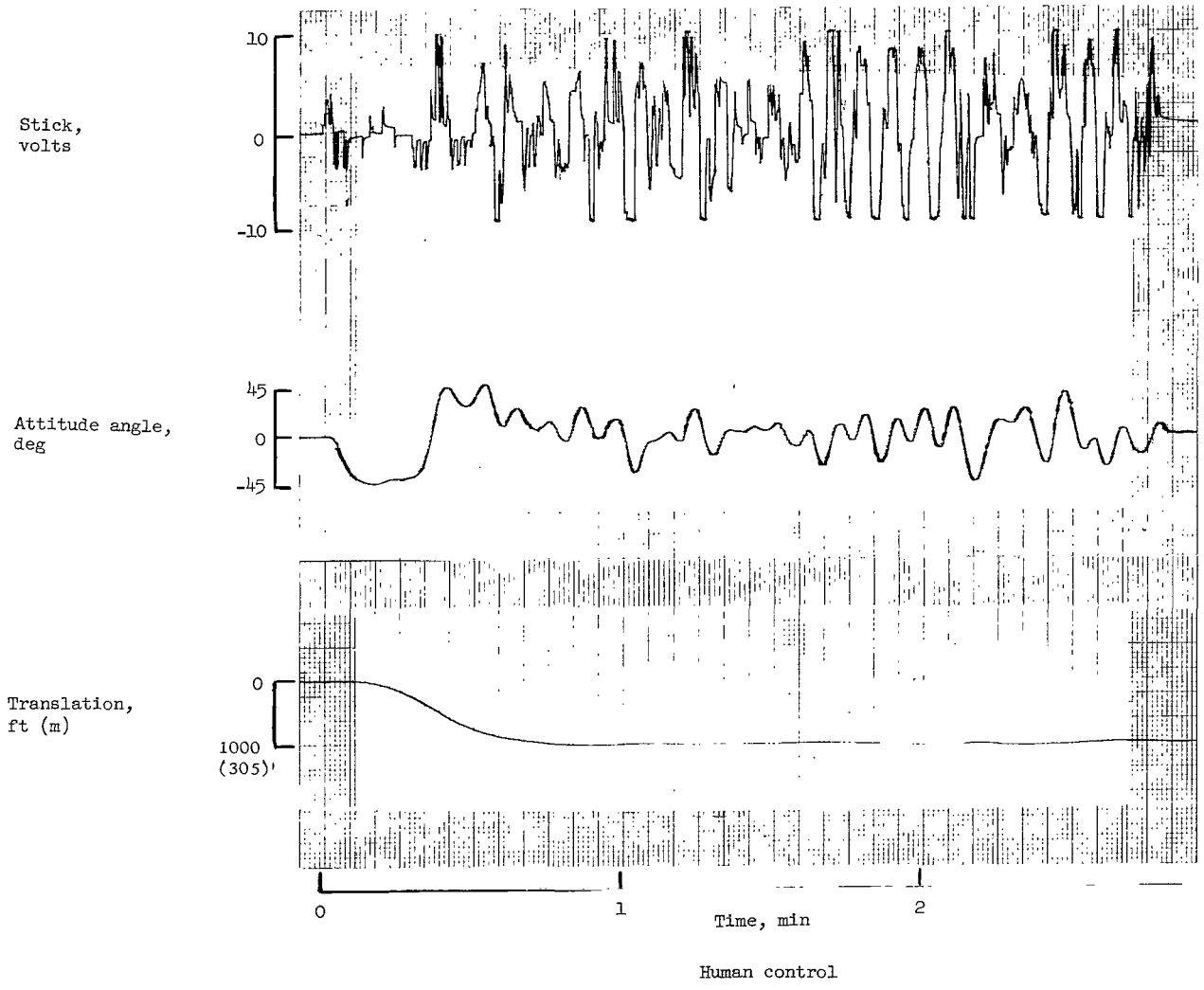

Figure 16.- Double-loop run with dynamics of $\frac{K_3}{s^2(s+1)}$ in inner loop, $\frac{K_3}{s^2}$ in outer loop.

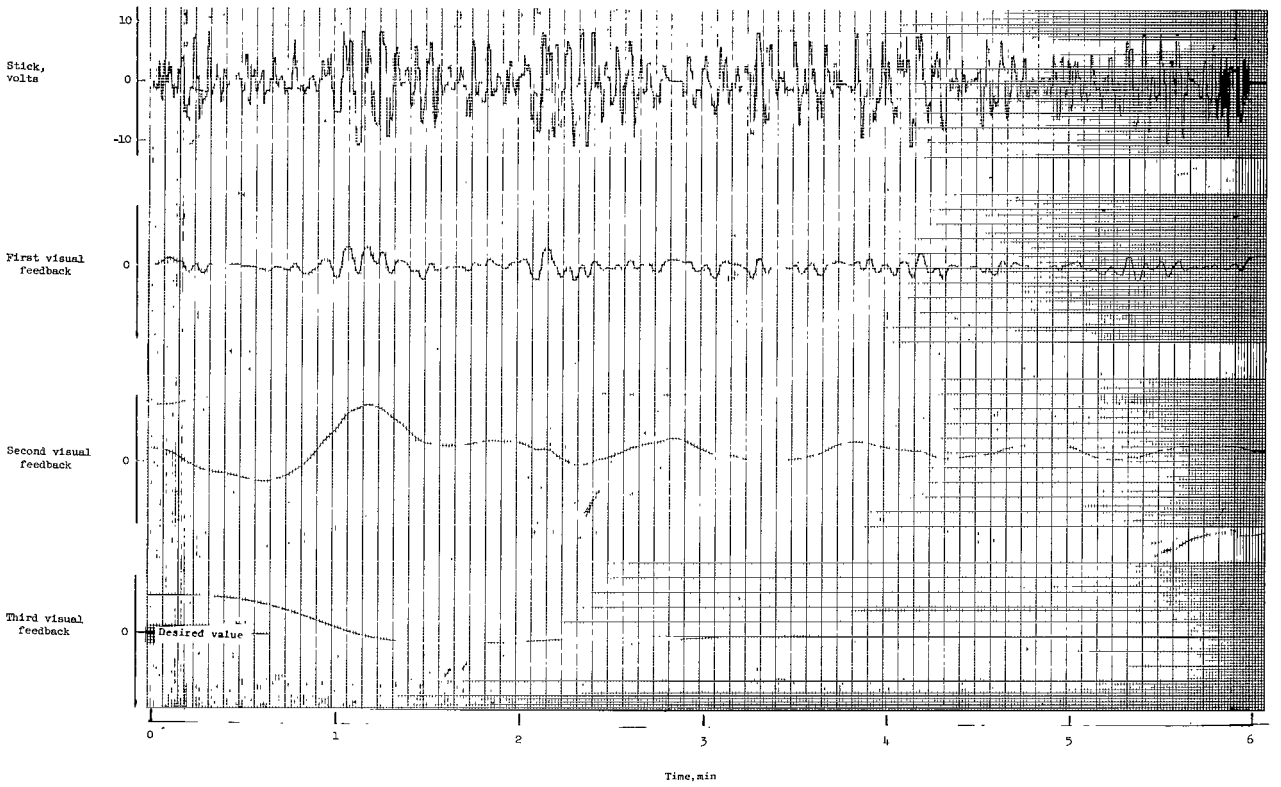

Figure 17.- Triple-loop run with $\frac{K}{s^2}$ dynamics in each loop.

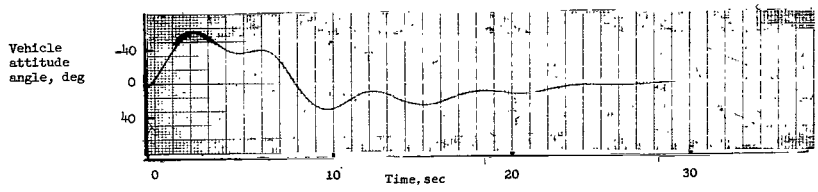

(i) Vehicle alone.

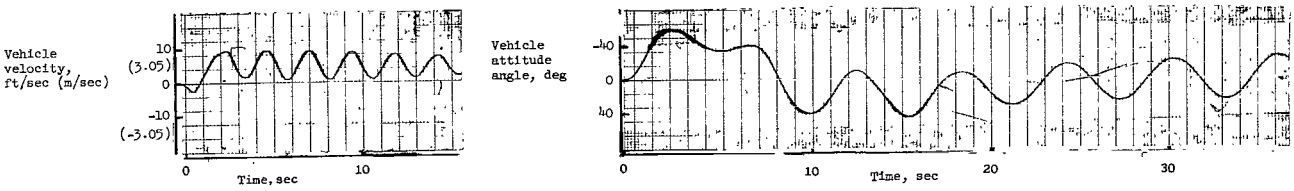

(ii) Response with high gain in simulator drive mechanism.

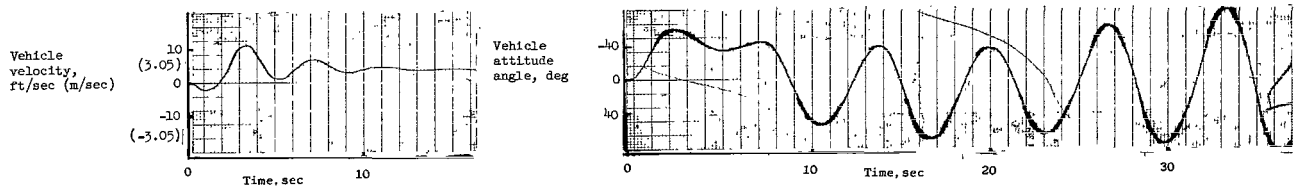

(iii) Response with low gain in simulator drive mechanism.

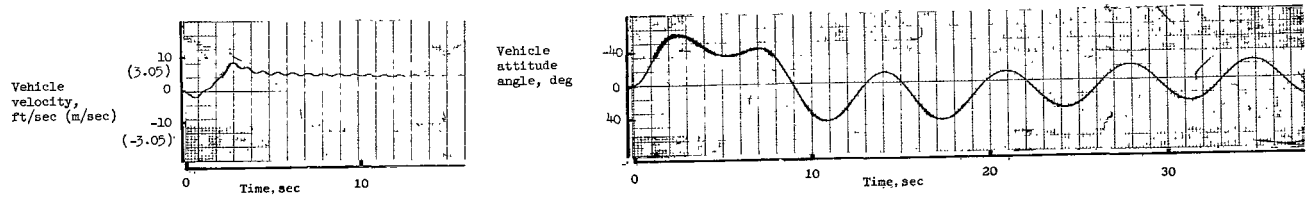

(iv) Response with alternate simulator drive system.

(a) 2-second step thrust input.

(b) Calculated pilot controlled 200-foot translation.

Figure 18.- Comparison of response characteristics of simulator to step thrust and pilot controlled maneuver.

"The aeronautical and space activities of the United States shall be conducted so as to contribute . . . to the expansion of human knowledge of phenomena in the atmosphere and space. The Administration shall provide for the widest practicable and appropriate dissemination of information concerning its activities and the results thereof."

—NATIONAL AERONAUTICS AND SPACE ACT OF 1958

NASA SCIENTIFIC AND TECHNICAL PUBLICATIONS

TECHNICAL REPORTS: Scientific and technical information considered important, complete, and a lasting contribution to existing knowledge.

TECHNICAL NOTES: Information less broad in scope but nevertheless of importance as a contribution to existing knowledge.

TECHNICAL MEMORANDUMS: Information receiving limited distribution because of preliminary data, security classification, or other reasons.

CONTRACTOR REPORTS: Technical information generated in connection with a NASA contract or grant and released under NASA auspices.

TECHNICAL TRANSLATIONS: Information published in a foreign language considered to merit NASA distribution in English.

TECHNICAL REPRINTS: Information derived from NASA activities and initially published in the form of journal articles.

SPECIAL PUBLICATIONS: Information derived from or of value to NASA activities but not necessarily reporting the results of individual NASA-programmed scientific efforts. Publications include conference proceedings, monographs, data compilations, handbooks, sourcebooks, and special bibliographies.

Details on the availability of these publications may be obtained from:

SCIENTIFIC AND TECHNICAL INFORMATION DIVISION

NATIONAL AERONAUTICS AND SPACE ADMINISTRATION

Washington, D.C. 20546